
Karl Christian Lautenschläger

Suitability of Modern Wi-Fi for Wireless-Infield-Communication of Agricultural Machines

Diploma Thesis in Information Systems Engineering

24 April 2023

Please cite as:

Karl Christian Lautenschläger, "Suitability of Modern Wi-Fi for Wireless-Infield-Communication of Agricultural Machines,"
Diploma Thesis (Diplomarbeit), Faculty of Computer Science, TU Dresden, Germany, April 2023.

Suitability of Modern Wi-Fi for Wireless-Infield-Communication of Agricultural Machines

Diploma Thesis in Information Systems Engineering

vorgelegt von

Karl Christian Lautenschläger

geb. am 29. Juni 1998
in Magdeburg

angefertigt an der

Technischen Universität Dresden
Fakultät Informatik
Networked Systems Modeling

Betreuer: **Christoph Sommer**
Gutachter: **Christoph Sommer**
Burkhard Hensel

Abgabe der Arbeit: **24. April 2023**

Erklärung

Ich versichere, dass ich die Arbeit ohne fremde Hilfe und ohne Benutzung anderer als der angegebenen Quellen angefertigt habe und dass die Arbeit in gleicher oder ähnlicher Form noch keiner anderen Prüfungsbehörde vorgelegen hat und von dieser als Teil einer Prüfungsleistung angenommen wurde.

Alle Ausführungen, die wörtlich oder sinngemäß übernommen wurden, sind als solche gekennzeichnet.

Declaration

I declare that the work is entirely my own and was produced with no assistance from third parties.

I certify that the work has not been submitted in the same or any similar form for assessment to any other examining body and all references, direct and indirect, are indicated as such and have been cited accordingly.

(Karl Christian Lautenschläger)

Dresden, 24 April 2023

Abstract

Wireless-Infield Communication (WIC) describes a wireless data exchange between agricultural machines in the field. A prototypical use case is an Agricultural Platooning Service, which exchanges guidance data positions following vehicles in a platoon with a lateral and longitudinal offset to a leading vehicle in the field. This thesis investigates the suitability of modern Wi-Fi for WIC based on the use case Agricultural Platooning Service. I analyzed process data and derived requirements of Agricultural Platooning Services in the corn harvest scenario.

Field measurements in an agricultural environment indicated that Wi-Fi communication can range up to 2500 m in a line-of-sight scenario. However, signal strength can suffer from multipath, shadowing and fading effects due to the agricultural environment and the machine sizes.

I simulated different Wi-Fi physical layer configurations that reduce the data rate but enable robust communication to overcome these challenges. The results enable configuration for long-range service discovery and Uniform Guidance Data exchange modes in the Agricultural Platooning Service. Finally, it was shown that the required latencies and message intervals for Agricultural Platooning Services could be met in the corn harvest scenario.

Kurzfassung

Gleicher Text (sinngemäß, nicht wörtlich) in Deutsch

Contents

Abstract	iii
Kurzfassung	iv
1 Introduction	1
2 Fundamentals	3
2.1 Wireless-Infield Communication	3
2.2 Use Cases for Wireless-Infield Communication	5
2.3 Wireless Lans according to IEEE 802.11	8
2.4 Related Work	20
3 Analyzing Agricultural Platooning Service Requirements	24
4 Field Measurements	32
4.1 Trial Run	35
4.2 Wi-Fi Range Measurements	37
4.3 Field Measurements Evaluation	39
5 Link Level Simulation	41
5.1 Robustness	41
5.2 Data Rate	51
5.3 Link Level Simulation Evaluation	60
6 Application Level Simulation	61
6.1 Agricultural Platooning Services	61
6.2 Application Level Simulation Evaluation	70
7 Conclusion	74
Bibliography	83

Chapter 1

Introduction

With the growing demand for increased efficiency and autonomy in the agricultural domain, Wireless-Infield Communication (WIC) has emerged as a key technology to improve the automation and digitalization of farming processes. WIC describes a wireless connection between agricultural machines in the field that enables process data exchange.

Given that there are many agricultural technology companies worldwide, and a mix of their machines often cooperate in individual agricultural companies, demand for interoperability between agricultural machines of different brands has emerged. In 2008, the Agricultural Industry Electronics Foundation (AEF) was founded to develop and standardize this interoperability¹.

The AEF is known for developing the ISO 11783 standard, a bus communication system between agricultural machinery, mainly tractors and implements [1]. According to Schlingmann and Benishek [2], the ISO 11783 standard is named ISOBUS system.

The authors mention that the AEF is currently working on other issues. Among them is also WIC. The associated project group WIC develops and standardizes solutions for Machine-To-Machine (M2M) wireless communication between cooperating agricultural machines.

In order to implement WIC, the WIC project group has been searching for a suitable technology that can realize the required data rates, latencies, robustness, and high transmission range. The plans to implement WIC are written down by Schlingmann et al. [3], members of the WIC project group. The authors consider the fundamental use of cellular networks as very problematic because, according to [4], only 30 % of the land surface has network coverage. For this reason, one major concern is that the required data cannot be exchanged because there is no network

¹<https://www.aef-online.org/about-us/about-the-aef.html>

connectivity around many fields. Nevertheless, the authors want to leave the future WIC system open to cellular standards.

The authors' current focus is on Wi-Fi technologies, especially IEEE 802.11p.

As of July 2021, the frequency spectrum of IEEE 802.11p in the United States of America, ranging from 5.85 GHz...5.925 GHz, has been split. The upper 30 MHz are reserved for Intelligent transportation systems now. The lower 45 MHz have been released for unlicensed operations [5].

Since the use of IEEE 802.11p has now been partly limited by the US Federal Communications Commission, the WIC project group is looking for an alternative Wi-Fi technology that enables WIC.

In this thesis, I intend to support the progress of the WIC project group and investigate how modern Wi-Fi can enable WIC. In particular, I will focus on the current Wi-Fi standard, IEEE 802.11ax. During my research, I will study the use cases of WIC in agriculture and the requirements and challenges for WIC in agriculture. To analyze the suitability of IEEE 802.11ax to enable WIC, I will concentrate on the example use case Agricultural Platooning Service. Agricultural Platooning Service enables the exchange of process data to guide a vehicle in a platoon with a lateral and longitudinal offset to a leading vehicle.

In the beginning, I will analyze agricultural process data to find the requirements and challenges of the mentioned use case. I will complement these with insights from past research on WIC in agriculture and wireless technologies in the agriculture domain in general.

The suitability of IEEE 802.11ax for WIC depends on whether the required data rates, latencies, high transmission ranges and robustness in the harsh agricultural environment can be achieved.

By understanding past limitations of Wi-Fi technologies for outdoor communication networks and exploring how IEEE 802.11ax addresses these limitations, I will investigate how IEEE 802.11ax can be configured.

For this purpose, I will conduct field experiments to detect the influence of the agricultural environment on the robustness and range of IEEE 802.11ax. As all physical layer parameters of IEEE 802.11ax are configurable, I will simulate how the capabilities of IEEE 802.11ax affect the data rate and the robustness of the wireless connection. After learning suitable parameter settings for the physical and MAC layer of IEEE 802.11ax, I will simulate the use case Agricultural Platooning Service to determine whether the requirements and challenges can be met by IEEE 802.11ax.

Chapter 2

Fundamentals

2.1 Wireless-Infield Communication

Since 2014, the WIC project group has been working on the development of a WIC standard, which covers a standard for machine-to-machine communication, encryption, and security². Schlingmann and Benishek [2] summarize the goals of the WIC project team as follows:

- Define use cases for WIC in agriculture
- Evaluate the suitability of communication technologies
- Find suitable communication protocols
- Standardize the WIC common software library
- Develop functional and security requirements and concepts
- Test first prototypes in regard to cross-brand conformance
- Write an application guideline

First steps have already been taken in this direction. The use cases and key scenarios are defined and explained by the authors as follows:

- **Real-Time Machine-to-Machine Control** is the exchange of control data under real-time conditions with defined latency policies. This use case enables leader-follower scenarios where agricultural machines follow a leading agricultural machine at a lateral and longitudinal distance. Throughout this thesis, I will refer to Real-Time Machine-to-Machine Control as Agricultural Platooning Service.

²<https://www.aef-online.org/about-us/teams.html>

- **Streaming Services** are communications that stream video from remote cameras and monitors at a high data rate and low latency. The authors estimate the distance between the communication participants to be less than 100 m. As a result, this data is available on another agricultural vehicle and can be analyzed and processed there. I will refer to Streaming Services as Agricultural Streaming Services in this thesis.
- **Process Data Exchange** describes the exchange of process data. One example is the exchange of already sprayed field areas to prevent multiple spraying of fertilizers and pesticides on the same field area by different machines. According to the authors, this WIC use case requires long-range technologies because agricultural fields worldwide can be vast.
- **Fleet Management & Logistics** is the potential retrieval of data from the ongoing agricultural process. This information can influence economic or agronomic decisions of agricultural enterprises or service companies and is therefore required in a Farm Management Information System (FMIS). Since not all agricultural machines may be connected to the FMIS, the WIC project group is looking at how to use M2M communications to bridge the missing communications infrastructure until the data reaches a machine that can connect to the FMIS.
- **Road Safety** describes a use case which is already a project between the European Telecommunication Standard Institute and the AEF. Since agricultural vehicles are repeatedly underestimated in their size and speed by other road users when they suddenly turn off the field onto the road, the other road users need to be warned in this situation. In this way, smart technologies in cars and motorcycles can brake these vehicles in advance and prevent possible accidents.

Considering that I investigate the suitability of modern Wi-Fi for Wireless-Infield-Communication and modern Wi-Fi like IEEE 802.11ax is no long range technology, I will focus on investigating the suitability of IEEE 802.11ax for the WIC use case Real-Time Machine-to-Machine Control. Throughout this thesis, I will refer to real-time machine-to-machine control as Agricultural Platooning. An example how farmers can benefit from Streaming Services or Agricultural Platooning Services is the corn harvesting and loading process.

2.2 Harvest and Loading Processes as Use Cases for Wireless-Infield Communication

The Forage Harvester (FH) has proven to be an essential agricultural machine for harvesting and loading forage. Seifert, Grimm, and Schurig [6] define a forage harvester as an agricultural loading machine for nearly all types of animal feed. According to the authors, a forage harvester can load the following animal feed by mounting different cutting and loading devices: Hey, Straw, Corn, Grass and Clover.

Ref: Photograph from CLAAS KGaA mbH

In the harvesting and loading process, a Transport Machine (TM) typically drives alongside or behind the FH so that the FH can load the harvested goods onto the trailer of the TM using the spout. Drivers operate both machines and try to keep the speed and distance so that the spout throws the harvested goods into the trailer of the TM. An image of a corn harvesting and loading process can be seen in Figure 2.1.

Taking a corn harvest scenario as an example, some key figures are represented in [7], a standard reference book in agricultural literature. This book contains key figures on farming processes, which 80 experts have compiled. The key figures, which are shown in Table 2.1, are dependent on the Plant Density (PD) and show the large amount of forage harvested by a FH every hour.



Figure 2.1 – Forage Harvester (FH) and Transport Machine (TM) in a corn harvesting and loading process

Plant Density (PD)	20 t/ha	30 t/ha	50 t/ha
Required Transport Machine (TM)	5	7	10
Harvested volume in m ³ /h	285.7-333.3	428.6-500.0	595.7-695.0
Filled Transport Machine loads in 1/h	5.7 - 6.7	8.6 - 10.0	11.9 - 13.9
Harvested mass in t/h	100	150	208.5

Table 2.1 – Key figures of corn harvest of a Forage Harvester (FH) with a working width of 6.2 m in a 80 ha-field in regards to Plant Density (PD) calculated from [7]

The harvesting and loading processes are examples of the use of agricultural Platooning Services as described by Zhang et al. [8]. This Platooning Service creates a leader and follower system where an uncrewed agricultural machine follows a leading operated agricultural machine. The operated FH, as a leader, sets the path and speed and transmits the data via WIC to the TM. Based on the path and speed data of the FH, TM follows unmanned with a longitudinal and lateral offset, as Figure 2.2 displays.

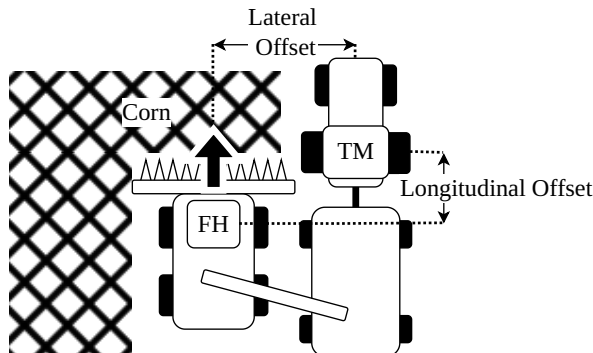


Figure 2.2 – Lateral and longitudinal offset between the two agricultural machines Forage Harvester (FH) and Transport Machine (TM) in a corn harvest scenario

The application of platooning services offers many advantages. The TM is positioned optimally to the FH so that the forage can be loaded ideally from the FH onto the TM.

Because, as displayed in Figure 2.3, fewer and fewer workers are working in agriculture, platooning services for harvest and loading processes can save and free up labour for other activities [9]. As stated in Table 2.1, ten drivers for the TMs are needed in the corn harvest process with a high PD. Using an Agricultural Platooning

Service, each TM can drive unmanned in the field, leading to fewer workers needed in the corn harvest process.

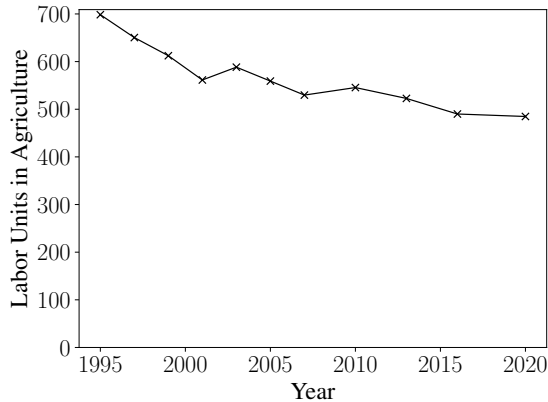


Figure 2.3 – Decrease in the agricultural labor force in Germany based on the data from [10]

Smolnik and Lücke [11] adds that platooning services at the platoon level can reduce FH drivers' workload so that they can focus on optimally adjusting the machines. In addition, TMs can be guided to the FHs in a targeted manner so that logistics processes in the field can be improved.

At the same time, the harvest and loading processes are examples of the video streaming WIC use case. During these harvest and loading processes, the spout of the FH must be controlled to set the loading position of the forage into the trailer of the TM.

According to Murcia [12], different spout guidance and control systems have been developed to automate the filling of the trailer. Spout guidance and control systems use a camera attached to the spout to determine the fill volume at each point of the trailer via machine vision and set the spout to fill the empty parts accordingly. The author describes Autofill from CLAAS and Intellifill from CNH Industrial as examples of spout guidance systems.

Streaming the video of a camera at the spout from the FH to the TM would be a practical application of the video streaming use case in the harvesting process. If the TM driver can watch a live stream of the trailer's fill level, he will always be informed and knows when the trailer is fully loaded and can drive the forage back to the farm.

2.3 Wireless Lans according to IEEE 802.11

According to Kauffels [13, p. 41], the first version of the Standard IEEE 802.11 was published in 1999 to enable a wireless alternative to Ethernet - or Token-Ring - networks. Sauter [14, pp. 265–268] considers IEEE 802.11 also to be an implementation of Ethernet with the help of wireless radio technologies. The author lists the extensions to the original standard, which range from 802.11b, 802.11g, 802.11a, 802.11n, 802.11ac to the latest enhancement 802.11ax. The different IEEE 802.11 standards can operate in the 2.4 GHz - , 5 GHz and 6 GHz - frequency band. IEEE 802.11n is also known as High-Throughput (HT) Wi-Fi [39], IEEE 802.11ac as Very-High-Throughput (VHT) Wi-Fi [15] and IEEE 802.11ax as High-Efficiency (HE) Wi-Fi [16]. The standards are acknowledged by these names. In addition, they are also called Wi-Fi 4, Wi-Fi 5 and Wi-Fi 6 respectively. Jacob et al. [17] adds that there are also two extensions IEEE 802.11p and its successor IEEE 802.11bd. These operate in a reserved frequency spectrum for Vehicle-to-everything (V2X) according to the authors in the 5.9 GHz frequency spectrum.

Kauffels [13, pp. 42, 43, 178–180] defines the following three basic architectures for IEEE 802.11.

If two or more stations (STAs) communicate directly without an Access Point (AP), they form an ad hoc network. According to the author, this can be set up quickly and easily and is called Independent Basic Service Set (IBSS).

The Infrastructure Basic Service Set (BSS) mode allows all STAs within the range of defined range around the AP to communicate via a central AP. Within the area of the BSS, all stations can move freely and communicate with one another.

Since an AP has limited range and can only cover a certain area, the Extended Service Set (ESS) was introduced. It contains a distribution system, which links several BSS with each other.

Thereby, the BSS coverage areas can physically overlap so that continuous connection of stations within the ESS can be provided. For a better performance the BSS can be physically placed on top of each other. One can also have objectively separate BSSs so that these BSSs can be linked together over long distances. According to the author, the standard does not specify a distance limit for such connections.

He also mentions that the standard defines the following three mobility types for station in an ESS, where a station can do no-transition and thereby stay within a BSS, BSS-transitioning and move from one BSS to another BSS within the same ESS and ESS-transition, where the Station moves from an ESS to another one but no stable connection can be guaranteed.

Sauter [14, pp. 272, 273] adds that usually Ethernet is used to link APs within an ESS. But according to the author this can be replaced by a wireless connection, which is called wireless bridge.

To enable communication between Wi-Fi devices, the IEEE 802.11 standard defines the physical and the MAC layer of the OSI model. The first layer is the physical layer.

Wi-Fi Physical Layer

A constant change of the physical layer accompanies the further development of IEEE 802.11. Sauter [14, p. 286] mentions that all new enhancements of the physical layer of IEEE 802.11 are backward compatible with previous definitions of the standard.

According to the Author, IEEE 802.11 initially used Direct Sequence Spread Spectrum and Frequency Hopping Spread Spectrum as modulation methods. Since IEEE 802.11g the modulation method Orthogonal Frequency-Division Multiplexing (OFDM) can be used in the 2.4 GHz frequency band. The author explains OFDM as follows. OFDM divides the transmission channel into subcarriers with different amplitudes, frequencies and phases. All subcarriers send data in parallel. Each subcarrier is orthogonal to another one, which means that the subcarriers do not interfere with each other.

Symbol length

The data is then sent as OFDM symbols over the individual OFDM subcarriers. The distance between subcarriers is specified as subcarrier spacing and corresponds to the reciprocal symbol length. IEEE 802.11ax increased the OFDM symbol length from $3.2 \mu\text{s}$ for IEEE 802.11n to a maximum of $12.8 \mu\text{s}$ [14, pp. 294, 310]. This corresponds to a subcarrier spacing of 312.5 kHz and 78.125 kHz respectively [14, p. 310].

For the IEEE 802.11p and IEEE 802.11bd standards, a symbol length of $6.4 \mu\text{s}$ applies, corresponding to a subcarrier spacing of 156.25 kHz [17].

The Fast Fourier Transform and Inverse Fast Fourier Transform are used to modulate and demodulate the transmitting bits. With the reduction of subcarrier spacing, more subcarriers are created in the transmission channel, so the Fast Fourier Transform size must be increased.

Kauffels [13, p. 132] adds that OFDM can be used in the 5 GHz frequency band since IEEE 802.11a.

Bandwidth (BW)

The frequency bands are divided into channels in order to create several transmission channels. This results in 13 channels in Europe in the frequency band of $2.412 \text{ GHz} \dots 2.482 \text{ GHz}$ and 18 channels in the frequency band of $5.180 \text{ GHz} \dots 5.350 \text{ GHz}$ and $5.470 \text{ GHz} \dots 5.725 \text{ GHz}$ [14, p. 274]. Transmission

channels can be combined to enable higher data rates. Every channel has a width called BW specified in MHz. The possible BWs for the IEEE 802.11 standards are shown in Table 2.2.

Standard	Channel BWs in 2.4 GHz	Channel BWs in 5 GHz	Channel BWs in 5.9 GHz
IEEE 802.11n [14, p. 299]	20 MHz, 40 MHz	20 MHz, 40 MHz	-
IEEE 802.11ac [15]	-	20 MHz, 40 MHz, 80 MHz, 160 MHz	-
IEEE 802.11ax [16]	20 MHz, 40 MHz	20 MHz, 40 MHz, 80 MHz, 160 MHz	-
IEEE 802.11p [17]	-	-	10 MHz
IEEE 802.11bd [17]	-	-	10 MHz, 20 MHz

Table 2.2 – Available BWs for the IEEE 802.11 standards per frequency band.

IEEE 802.11ac and IEEE 802.11ax also enable the use of a discontinuous BW, which combines two 80 MHz channel to a 160 MHz BW channel [16], [15].

While wider channels increase the theoretical data rate, Avallone et al. [18] mentions that narrower channels can boost the signal's power spectral density and thus increase the transmission range.

Modulation and Coding Scheme (MCS)

In order to encode as many bits as possible on one OFDM symbol, different MCSs can be used. The MCSs for the IEEE 802.11 standards are based on Phase Shift Keying (PSK) or Quadrature Amplitude Modulation (QAM) [14, p. 305]. The smallest MCS is Binary - PSK and encodes 1 bit per symbol [13, p. 140], [14, p. 304]. IEEE 802.11ax increases the most complex MCS from 256 - QAM at IEEE 802.11ac to 1024 - QAM and thus now encodes 10 bit per symbol [19]. In the V2X standards IEEE 802.11p and IEEE 802.11bd, the MCSs can range from binary - PSK to 256 - QAM [17].

An imaginary, theoretical transmission channel is usually specified as a square-wave signal in the frequency domain with limits of both minimum and maximum amplitude and cut-off frequency. Kauffels [13, pp. 158, 159] defines the roll-off factor as a cosine-shaped flattening of the square signal between 0 and 1. In addition, the author points out that QAM can generate high roll-off factors so that signals interfere significantly more with adjacent channels.

In this regard, the author recommends setting the parameters in an OFDM system so that first, the coding rate and then the complexity of the MCS is reduced in challenging transmission environments. The more bits a MCS encodes on a symbol, the more error-prone the correct decoding.

Forward Error Correction (FEC)

Nevertheless, bit errors can occur during transmission. In this regard, Kauffels [13, p. 135] mentions and explains FEC as a technique to reduce bit errors during transmission. FEC adds redundant bits to the data. The receiver uses these redundant bits to check the integrity or correct errors of the received data. The proportion of non-redundant transmission bits is defined in the Coding Rate (CR).

To achieve this, binary convolutional coding (BCC) is used mandatory since the IEEE 802.11n standard [19], [20]. Syafei et al. [20] add that it is optionally possible to use low-density parity-check (LDPC). The authors state that LDPC can achieve a better channel capacity performance. This impact is also confirmed by Afaqui, Garcia-Villegas, and Lopez-Aguilera [19], who point out that LDPC also generates higher computational cost.

IEEE 802.11ax stations must support LDPC when using the IEEE 802.11ax standard under the following conditions [16], [19] :

- The used bandwidth is greater than 20 MHz
- The chosen MCS is 1024-QAM
- More than four transmission channels are used for the transmission.

IEEE 802.11ax achieves CR of $1/2$, $2/3$, $3/4$, and $5/6$ [16]. Similarly, IEEE 802.11p uses the BCC technique, which has been superseded by LDPC in its successor IEEE 802.11ax [17], [21]. Yacheur, Ahmed, and Mosbah [21] argue that this step was important, as LDPC offers better error correction possibilities for higher communication ranges greater than 50 m.

Together with the MCS, the FEC CR form a physical layer specification, which is named after the specific standard. For IEEE 802.11ax, this results in the HE-MCS values in Table 2.3.

Guard Interval (GI)

Pulimamidi, Nulu, and Tahernehzadi [22] describe the Guard Interval as a cyclic prefix of OFDM symbols to prevent intersymbol - and intercarrier interference. Intersymbol interference is caused by multipath delays, where the reflected delayed previous symbol can interfere with the currently received symbol [23]. Similarly,

HE-MCS index	Modulation and Coding Scheme (MCS)	Coding Rate (CR)
0	Binary PSK	1/2
1	Quadrature PSK	1/2
2	Quadrature PSK	3/4
3	16-QAM	1/2
4	16-QAM	3/4
5	64-QAM	2/3
6	64-QAM	3/4
7	64-QAM	5/6
8	256-QAM	3/4
9	256-QAM	5/6
10	1024-QAM	3/4
11	1024-QAM	5/6

Table 2.3 – MCS and CR for HE-MCS values [16]

intercarrier interference is caused by time-varying channel resulting in a longer OFDM symbol duration [24].

Pulimamidi, Nulu, and Tahernehzadi [22] explain how a guard interval can prevent these interferences. Since the guard interval is designed to prevent possible interference on the following symbol, it must be at least long enough to catch all channel impulse responses with the resulting delays. The guard interval is then removed again at the receiver. This results in an attenuation of bandwidth which can be described by the authors with the following formula:

$$\text{GI_Bandwidth_Attenuation in \%} = \frac{\text{OFDM_symbol_duration} \times 100 \%}{\text{OFDM_symbol_duration} + \text{GI}}. \quad (2.1)$$

Since IEEE 802.11n, a shortened GI of 400 ns is usable, which increases the maximum data rate from 270 Mbit/s to 300 Mbit/s compared to the usual GI of 800 ns [14, pp. 294, 296]. IEEE 802.11ax supports GIs of 800 ns, 1600 ns and 3200 ns to enable better protection against multipath effects in indoor and outdoor communications [25].

No condition for the use of the different GI is mentioned in [25], [26], [27] or [19]. Moreover, the sources mentioned only specify a OFDM symbol length of 12.8 µs.

Nevertheless, the standard IEEE 802.11ax [16] specifies the following rules for using the different GIs. A 1600 ns GI can only be used with a symbol length of 6.4 µs. The same applies to a GI of 800 ns, with the optional extension for use with a symbol length of 3.2 µs. A GI of 3200 ns can only be used for a symbol length of 12.8 µs.

Multiple Input Multiple Output (MIMO)

In order to further exploit the physical layer capabilities, the single transmitting and receiving antenna systems called Single-Input-Single-Output can be extended to MIMO - systems. Sauter [14, pp. 294–296] describe the idea behind MIMO as the usage of multiple transmit antennas and multiple receiving antennas. Spatial multiplexing is used so that the transmitted signals from each antenna are reflected differently on objects and can thus be received from different directions at the receiver antennas.

The authors explain that since IEEE 802.11n, it is possible to use up to 4 MIMO streams. This number was increased again up to 8 MIMO streams in IEEE 802.11ax [16]. Since data can be sent simultaneously via each MIMO stream, the theoretical data rate can thus increase proportionally depending on the usable streams. The mechanism is called Single-User (SU)-MIMO [16].

Sauter [14, p. 308] mentions that since IEEE 802.11ac it is possible to use Downlink Multi-User (MU)-MIMO, which allows an AP to transmit data to multiple STAs via different available MIMO streams simultaneously. According to the authors, MU-MIMO can increase the network throughput. IEEE 802.11ax introduced MU-MIMO in the Uplink direction [16], where multiple STAs can transmit data simultaneously to the AP via different available MIMO streams.

Another MIMO technique is Orthogonal Frequency-Division Multiple Access (OFDMA), which can be utilized since IEEE 802.11ax [16], [18], [29]. Avallone et al. [18] explains that OFDMA enables an AP to transmit data to multiple STAs simultaneously by dividing the available bandwidth into Resource Units (RUs) and assigning each RU to a STA. The authors add that OFDMA can be used in both the uplink and downlink direction. Every RU is defined with a number of OFDM subcarriers, which can transmit data within the RU. The AP can choose the best suited RU for each STA and thus increase the Signal-to-Interference-plus-Noise Ratio [30]. Behara and Venkatesh [31] adds that OFDMA is designed to improve the per-user throughput in high-density networks, e.g. stadiums, airports or public transportation systems.

Space-Time-Block-Code (STBC)

Abbas et al. [32] further explain that MIMO spatial streams can be utilized to enhance the quality of the received signal. The Technology is called STBC. Santumon and Sujatha [33] explain it as follows. STBC is a technique used in Wi-Fi networks to improve the reliability and robustness of wireless communications. STBC encodes multiple redundant copies of data at the transmit side, which are transmitted in different spatial streams to reduce fading and interference effects. At the receiver

side, these multiple copies are combined using a maximum likelihood detector to retain a high-quality signal and decrease the packet error rate (PER).

Here, Stamoulis and Al-Dahir [34] investigated the potential effect of STBCs on Wi-Fi. Their simulations showed that STBCs increase the range and robustness for IEEE 802.11a. In addition, the authors concluded that STBC increases the Signal Noise Ratio (SNR) in nearly all cases at the same throughput or even allows higher MCS values to be used, thus allowing a higher throughput at the same SNR. This results in STBC improving the reliability and robustness of wireless communications.

Ghosh et al. [35] analyzed the error rate performance for an increased number of used antennae and found that a lower bit error rate can be achieved when increasing the number of transmit antennas with STBC.

Gast [36, Chapter 4] and Sauter [14, p. 301] mention that STBC can extend the signal range due to the increased robustness.

IEEE 802.11ax stations can optionally use STBC under the following conditions [16]:

- Dual Carrier Modulation (DCM) is not applied
- The number of spatial streams is 2
- The GI is not 0.8 ns and the symbol length is not 12.8 µs

Gast [36, Chapter 8] states that STBC is only supported in 1/5 of the Wi-Fi-certified devices.

Dual Carrier Modulation (DCM)

To introduce additional robustness DCM can be applied to the physical layer since IEEE 802.11ax [17], [28], [16]. Jacob et al. [17] describe DCM as sending data twice over two coherent carriers. At the receiver, the data copies are combined with the log-likelihood ratio. Thus DCM increases the probability of receiving the data.

[16] provides a receiver minimum input sensitivity, which indicates until which Received Signal Strength (RSS) a packet is received with a probability of 90 %. The receiver minimum input sensitivity for a BW of 20 MHz is displayed in Figure 2.4. It demonstrates that when using DCM, the receiver minimum input sensitivity can be lower than without using DCM. The effect on the receiver minimum input sensitivity increases as the HE-MCS value increases.

A similar development of the receiver minimum input sensitivity can also be observed for higher BW, except that the lowest value increases with BW.

The higher probability of achieving data is reached at the expense of the data rate. The same amount of data now takes twice as long to transmit.

[16] lists the theoretically possible data rates. These reveal that the maximum achievable data rate with DCM is only half of the attainable data rate without DCM.

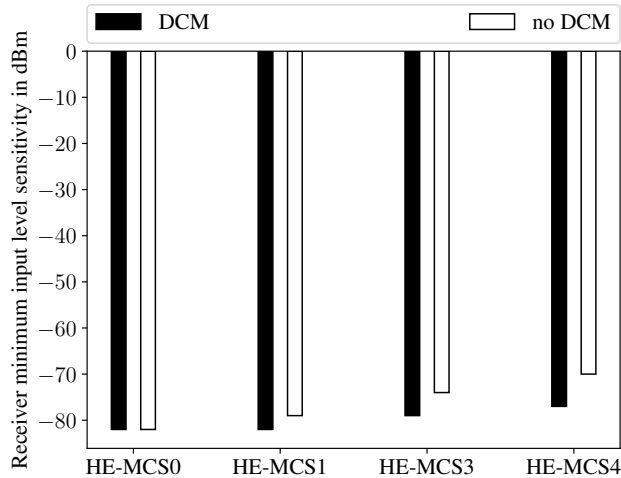


Figure 2.4 – Receiver minimum input level sensitivity for different HE-MCS values according to [16], where PER is less than 10 %

Support for DCM is only optional in the IEEE 802.11ax standard and can only be used for HE-MCS-0, HE-MCS-1, HE-MCS-3 and HE-MCS-4 for 1 or 2 spatial transmission streams, when STBC is not enabled [16].

MU-MIMO DCM can also be applied in IEEE 802.11ax [16].

Jacob et al. [17] and Triwinarko, Dayoub, and Cherkaoui [28] mention plans, to allow using DCM in the physical layer of IEEE 802.11bd.

Extended Range (ER)

Since IEEE 802.11ax, the ER Mode exists, which defines the new HE ER SU Physical layer convergence protocol data unit (PPDU) as physical layer amendment [16], [19]. Deng et al. [25] explains that the HE ER SU PPDU format is intended to extend the range of a single station to access point transmission. According to the authors, this is accomplished by the PPDU containing a repetition of the HE-SIG-A field.

In addition, the authors explain that the preamble transmission power is boosted to guarantee reliable transmission for longer ranges. The power-boost is limited to additional 3 dB in [16], [17].

The IEEE 802.11ax [16] standard defines that the HE ER SU PPDU format may only be used when 20 Mhz transmissions with either 242-RU with HE-MCS-0 - HE-MCS-2 or 106-RU with HE-MCS-0 are used on a spatial stream. In addition, one can use DCM. Sauter [14, p. 311] defines the RU as fragments of a Wi-Fi channel. The number before the RU indicates the number of subcarriers which are part of the RU.

Optionally, the HE ER SU PPDU may also be transmitted with a GI of 800 ns, where an additional application of DCM is forbidden.

Jacob et al. [17] and Triwinarko, Dayoub, and Cherkaoui [28] add that it is planned to use the ER mode also in the IEEE 802.11bd standard.

Wi-Fi Data Link Layer

The next layer in the OSI model is the Data Link Layer. The Data Link Layer consists of MAC and LLC functionalities.

According to Kauffels [13, p. 207], the MAC functionalities cover network entry, authentication, and media access methods. The author explains that every AP send beacon frames periodically to synchronise its stations in the BSS and that the beacon frame contains the Service Set Identifier (SSID), which identifies the BSS or ESS of the station. Sauter [14, pp. 275–276] adds that a beacon frame contains a 16 bit - long capability information element. Each bit here signals that the AP provides a particular function or has a specific feature.

What is LLC? Logic
Link Control?

Kauffels [13, pp. 220, 221] explains a station's network entry procedure. A station can use the passive or the active scanning mode. The station listens for a beacon frame in the various transmission channels in passive scanning mode. Alternatively, a station can send a probe frame in active scanning mode. The probe frame can either contain an already known SSID to test the presence of the AP or include a broadcast SSID that causes all nearby APs to respond. The response of an AP to the probe frame is the probe-response frame, which contains the same information as a beacon frame. With the information from the beacon frame, a station can start the authentication process.

For this process, Kauffels [13, pp. 221, 222] names the two methods Open System Authentication and Shared Key Authentication. Sauter [14, p. 277] explains that Open System Authentication is based on a device making an authentication request to the AP. If the AP answers with a positive status in the Authentication Frame, the station is included in the BSS. The actual encryption and authentication are then performed by the Wi-Fi Protected Access (WPA) functions. The author points out that Shared Key Authentication is no longer used today. Sommer and Dressler [37, p. 122] adds that the authentication process differs for the Ad-Hoc mode, where every station can authenticate new stations.

After the authentication process, the station receives a time-synchronisation function with a timestamp, the physical layer parameter configuration and the SSID of the BSS or ESS. The STA can start the media access method now.

The IEEE 802.11 standard describes the two media access methods Distributed Coordination Function (DCF) and Point Coordination Function (PCF).

Sauter [14, p. 283] explains that DCF is based on the media access method Carrier Sense Multiple Access/Collision Avoidance (CSMA/CA). In CSMA/CA, a device willing to transmit senses in the air transmission medium for a transmitting activity. If no other device is transmitting, the device can transmit. In transmitting activity, the terminal must wait at least until the transmission and the Interframe Space (IFS) are over. Various access priorities are implemented by different IFS lengths [37, p. 120].

Since data transmission via the air transmission medium is very vulnerable to errors, the standard IEEE 802.11 requires that each received unicast packet be confirmed with an Acknowledgement (ACK) frame [37, p. 120].

[add sources](#)

Sauter [14, p. 284] explains DCF IFS as the time after an transmission, which ensures that an ACK frame can be sent before another station uses the same channel to send a data frame. If the channel is busy, the station waits until the channel is free again. Sauter [14, pp. 284–285] describes this backoff procedure as follows: each ready-to-transmit device determines a random backoff time from a time interval called the contention window. The device with the shortest backoff time transmits next, and all other ready-to-transmit devices restart the media access procedure to avoid multiple devices transmitting simultaneously after Distributed Coordination Function Interframe Space (DIFS). If two devices start sending next because they randomly chose the shortest backoff time, the transmitted signal will interfere, and the packets will not be answered with an ACK frame. The author adds that in case of such a faulty transmission, the contention window increases exponentially until the maximum value of retries is reached and the contention window size is reset to the starting value.

To share the knowledge of a transmission time and the subsequently IFS, a packet contains a Network Allocation Vector (NAV) that specifies the time the air transmission medium is used [14, p. 284]. Collisions can occur as the NAV information can be reset by other transmissions from a different, overlapping network. To avoid this, IEEE 802.11ax maintains two NAVs, one for intra-BSS and one for inter-BSS transmissions [16]

The extension IEEE 802.11e introduced a amendment of CSMA/CA called Enhanced Distributed Channel Access (EDCA) [37, p. 121] [38]. According to Sommer and Dressler [37, p. 121], EDCA provides a Quality-of-Service transmission procedure, which classifies 4 access categories. Each access category has different minimum and maximum contention window sizes and different IFS lengths, named arbitration IFS. Wu et al. [38] explains that each access category keeps its own backoff counter and frame queue. Every access category is handled as an independent virtual station which tries to access the medium. When two transmissions of

different access categories collide, and both contention windows are set to zero simultaneously, the EDCA mechanism ensures that the access category with the higher priority wins.

The four access categories are listed in Table 2.4.

EDCA is integrated into the modern IEEE 802.11 standard data link layer of IEEE 802.11ac [15] and IEEE 802.11ax [16].

Access Category	Priority (1 = Highest)
Voice	1
Video	2
Best Effort	3
Background	4

Table 2.4 – Access Categories and their priorities for IEEE 802.11e EDCA [38]

In various network architectures, the "hidden station"-problem may occur. As you can see in Figure 2.5, Station A cannot sense a transmission of station B and vice versa. In case of simultaneous transmission of both stations, interferences around the AP may occur.

To prevent the hidden station problem, Sauter [14, pp. 282–283] explains that a STA can access the medium via the Request-to-Send (RTS)/acCTS mechanism. The STA sends a RTS frame to the AP and waits for a Clear-to-Send (CTS) frame. After receiving the CTS frame, the STA has reserved the medium for a specific time and can send its data frame. The successful transmission of the data frame is confirmed with an ACK frame. To avoid another STA accessing the medium during the RTS and CTS frames, the PCF IFS is shorter than the DCF IFS. This mechanism allows the AP to send the CTS frame before another STA can access the medium.

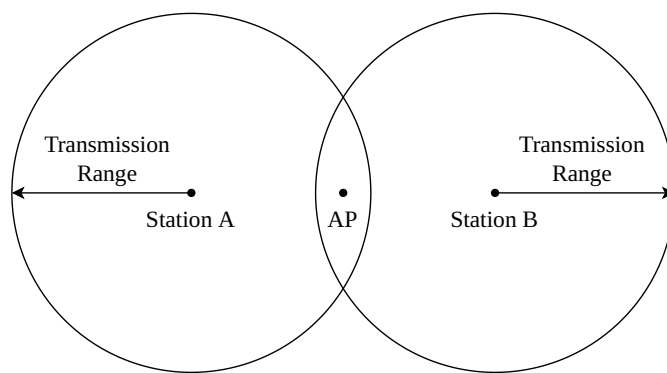


Figure 2.5 – Hidden Station Problem, where interferences at the Access Point (AP) can occur, when station (STA) A and B send simultaneously

Sauter [14, p. 283] states that the RTS/CTS mechanism is usually not configured because it introduces additional overhead of the RTS and CTS frames, which is only worth it when the data frame is large.

Larger frames can also be split into smaller frames to reduce the probability of collisions. This procedure, called fragmentation, divides the data into up to 16 frames when a specific data length threshold is exceeded [39]. The fragmented frames are transmitted by the three following different ACK policies in Figure 2.6, which are described by Sauter [14, pp. 334–335].

Using the standard ACK policy, the sender applies the DCF mechanism before sending each frame. The sender also waits for an ACK frame from the receiver after each transmission.

Instead of operating in the DCF mode, the sender can also send the next frame after waiting for the Short Interframe Space (SIFS) time when the ACK frame has been received. This is displayed in 2.6b and saves the overhead of acquiring the medium again.

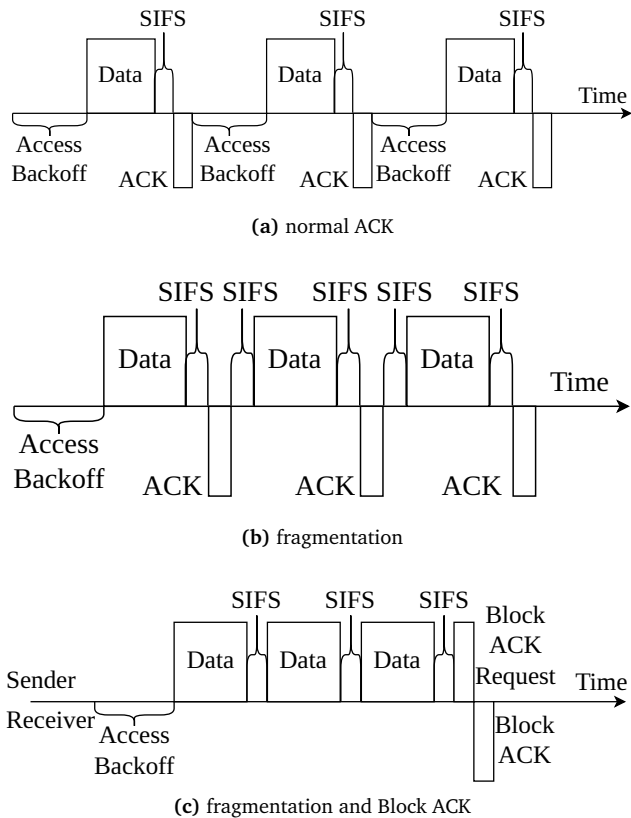


Figure 2.6 – Data transmission between a sender and receiver in regards to the time with normal Acknowledgement (ACK) 2.6a, fragmentation 2.6b and additional Block ACK 2.6c

Additional transmission time can be saved using the Block ACK policy, shown in 2.6c. The sender sends the first frame and waits for the ACK frame. After transmitting all fragments, the sender sends the Block ACK request. The receiver sends the Block ACK frame, which contains the information of all received frames. All missing frames are retransmitted. The Block ACK frame can be sent delayed when some processing time is required.

Every Block ACK session is started with an add Block Acknowledgment (ADDBA) request frame, which is sent by the sender and contains the session parameters. The receiver sends an ACK and answers with an add Block Acknowledgment (ADDBA) response frame. After the sender acknowledges the response frame, the Block ACK session is established. The Block ACK session is ended with a delete Block Acknowledgment (DELBA) frame, which is sent by the sender and acknowledged by the receiver.

The Block ACK policy can be used in IEEE 802.11n [39], IEEE 802.11ac [15] and IEEE 802.11ax [16]. In the IEEE 802.11p standard, the Block ACK policy can be added as an optional feature [40].

2.4 Related Work

Since my undergraduate thesis³ about *Wirelessly Networked Coordination of Automatic Section Control for Agricultural Machines*, I have been working on the topic of WIC. I conducted both field experiments and simulations to investigate the performance of LoRa as a technology to exchange process data in meshed Automatic Section Control, a prototypical application of connected vehicles in the agricultural domain. A summary of my results is published in a paper [41]. In my undergraduate thesis and paper, I described the current state of research in the field of WIC.

The first research paper on WIC that I found was from Ali et al. [42]. The authors developed a system based on General Packet Radio Service (GPRS) to exchange position data between TMs and combine harvesters to guide empty TMs to a combine harvester.

Smolnik and Lücke [11] describes the research project *5G Netmobil* in which the authors investigated how existing technologies like IEEE 802.11 or 3GPP LTE can be integrated into 5G technologies to enable Agricultural Platooning Services. The research plan was to evaluate the use of User Datagram Protocol (UDP) and Basic Transport Protocol (BTP) to exchange guidance data via the underlying technologies 3GPP LTE and 5G V2X and IEEE 802.11p. The authors implemented a system using 802.11p, as according to their technical analysis, this technology already fulfills the requirements for data rate, latency and the number of participants. The

³<https://github.com/klautenschlaeger/mvsc>

authors report that the project results demonstrated that achieved latencies were five times lower than the defined maximum latency of 50 ms for Agricultural Platooning Services.

Further research on WIC is not based on cellular networks. Zhang et al. [8] used IEEE 802.15.4 to implement a prototype of an Agricultural Platooning Service, where the developed system exchanges relevant control data between a leading tractor to guide a following tractor.

Smolnik and Lücke [11] states that the developed system of Zhang et al. [8] is part of the project *Elektronische Deichsel für landwirtschaftliche Arbeitsmaschinen (EDA)* and it was further improved within the scope of project *Elektronische Deichsel für landwirtschaftliche Arbeitsmaschinen mit Umfeldsensorik und zusätzlichen Geoinformationen (EDAUG)*.

Klingler, Blobel, and Dressler [43] investigated how IEEE 802.11p can be used for WIC. Experiments revealed that data could be exchanged over a maximum range of 1700 m, where Line-Of-Sight (LOS) was lost. But during the measurement in an agricultural work scenario from the corn harvest, there were collapses in the RSS due to shadowing effects of the machines. The authors point out that the size and shape of the forage harvester can cause intensified shadowing effects.

There are also more developments from the industry in the field of WIC. In this context, Thomasson et al. [44] describe the John Deere Machine Sync and Case IH V2V systems as follows:

John Deere Machine Sync enables the WIC use cases Process Data Exchange and Agricultural Platooning Service. Liu et al. [9] have extended the system to use Combine Harvesters, adding that the Machine Sync system is based on Metzler, Flohr, and Hoeh [45]'s patent. Smolnik and Lücke [11] adds that John Deere Machine Sync is only available for a subgroup of John Deere machine types and cannot be used with machines of other brands.

Case IH V2V also offers an agricultural platooning service. However, according to the authors, the system can only be used for harvesting and loading scenarios.

Also currently on the market is the Raven Autonomy™ Driver Assist Harvest Solution⁴ system from Raven Industries. This system allows the harvester to take control of a TM from a distance of 70 m. The harvester then automatically guides the TM into the perfect position to load the harvested crop onto the TM via the spout. Once the harvesting and loading process is complete, the driver of the TM driver retakes control.

A comparable system is CartACE from AgLeader⁵

The technology used in the mentioned systems is not known. In response to questions about how the systems can be used on farms worldwide and what

⁴<https://ravenind.com/products/autonomy/driver-assist-harvest-solution>

⁵<https://www.agleader.com/harvest/cartace/>

prerequisites must be created for this, the manufacturers refer to the regional distribution options.

Wireless communication technologies are also used to implement wireless sensor networks in the agricultural domain.

According to Ahmed, De, and Hussain [46], wireless sensor networks in the agricultural domain can be used to monitor soil and water conditions, plant diseases, and farm automation solution or track animals or assets. The authors mention similar requirements for wireless sensor network applications compared to WIC applications. For example, asset-tracking applications require low latency and must support asset mobility. The authors' results indicate that fog computing can lessen the latency and the required bandwidth compared to cloud computing. When a higher data rate is required, the authors recommend Wi-Fi technologies like IEEE 802.11n or IEEE 802.11ac.

As wireless sensor networks for agricultural applications, they must be able to operate in the same agricultural environment as WIC applications. Brinkhoff and Hornbuckle [47] describe that they expect a limited cellular network coverage and complex outdoor environments with large water areas, different crop vegetation, and other obstacles or various weather conditions. The researchers developed a wireless sensor network based on IEEE 802.11b, where they exchanged data between an AP and multiple stations on a cotton and rice field. The authors report that they easily achieved a communication range of 1000 m in a LOS scenario. They mention that different wheater conditions have little impact on communication reliability. A significant influence on the communication range is the height above ground or the crop vegetation, where the authors recommend using at least a height of 0.2 m.

Wi-Fi technologies are also used in various outdoor scenarios. The outdoor performance of Wi-Fi technologies in different use cases and scenarios have been investigated by various researchers. Aust, Prasad, and Niemegeers [48] surveyed past research on outdoor performance of IEEE 802.11 technologies. The authors summarize results of urban, rural, desert or water surface scenarios with different environmental conditions and antenna configurations. I focus on the findings for Wi-Fi with omnidirectional antennas in rural areas.

In their general findings, they cite [49] and [50], which name the intersymbol interference due to multipath effects as main reason for packet losses in Wi-Fi outdoor communication. The authors conclude, that using directional antennas instead of omnidirectional antennas can lead to fewer multipath effects. Furthermore, the authors add that external Wi-Fi interference is only expected in urban areas and is not very likely in rural areas.

Due to the experiment results of [51], the authors state that the weather conditions only have a small impact of 1 dB...2 dB on the outdoor communication. These findings are also confirmed by [47] in their experiments on a rice and cotton field.

Paul et al. [52] analyzed the open outdoor performance for different physical layer and MAC layer configurations of IEEE 802.11n. The authors conducted experiments with different omnidirectional antenna constellations and spacings ranging from 0 cm ... 25.4 cm. They found out that no positive impact on the communication can be achieved by changing antenna constellations or spacings.

For the MAC layer with its CSMA/CA mechanism,Aust, Prasad, and Niemegeers [48] state that the increased propagation delay in outdoor scenarios can cause a higher number of packet collisions. They refer to findings of [52] and recommend using Block Acknowledgement and Frame Aggregation. These mechanisms introduce a medium access control frame overhead, which cost less transmission time than retransmission of a whole frame or a single acknowledgment frame.

Chapter 3

Analyzing Agricultural Plowing Service Requirements

To gain a better insight into requirements of the WIC use case Agricultural Plowing Service, I analysed process data of a corn harvest scenario.

The goal of analysing the corn harvest data was to investigate the machines moving in the working scenarios relative to each other. The machines' speed and distance in tracked harvest platoon data may result in new use case requirements, e.g. latency or communication range. The machinery movement profile can be used to identify when shadowing effects may occur in the work scenario or when machines meet in the field.

To get GPS data of the corn harvest, I collected GPS tracks of a FH and two to three TMs harvesting corn on a field in Germany for two days in September. The workflow for collecting the corn harvest process data was as follows. I handed out the tablets to the drivers, which left the farm with the tablets in the driver's cabs to drive to the field in the morning. The tablets recorded the position and speed of the FH and the TMs every second of the day. During breaks, the tablets continued to capture the NMEA data stream of their GPS even if the positions and speed did not change.

After recording the process data, I anonymised it. First, I deleted data log lines of the log files until the recorded accuracy of the following data log lines was better than 2 m. Then, I replaced the timestamp and the date for all data points with a continuous index.

Then I anonymised the location data by adding a random offset to the GPS coordinates. As a result, this procedure moved the areas to a random location in the world with a continuous index as a timestamp, where the exact date is unknown.

To get a first glance at the recorded data, I built a dashboard with the Python framework *Dash*⁶. I initially plotted all the positions in a polyline for each machine on a map in the dashboard. An added slider allows one to set a time interval that narrows down the data points for display in the dashboard. In addition, one could select which TMs are displayed next to the FH. For the chosen time interval, the distance and velocity difference between the selected TMs and the FH were plotted in graphs as time histories. In the dashboard, I could get an overview of the machine's behaviour before, during, and after the overloading scenario. The overview shows that a FH is nearly always in the overloading process with a TM. In doing so, the FH may occasionally stay in the same place if the cutter is clogged or there is a transition of TMs where a full TM moves away from the FH and an empty TM catches up to the FH to take over the forage.

A TM is in a platoon with a FH if the distance to the FH is less 10 m and they are moving at nearly the same speed with a maximum velocity difference of 5 km/h (1.39 m/s). The distance between TM and FH increases during a turning manoeuvre on the field. Since both machines have different curve radii in a turning manoeuvre, a different machine speeds are required to finish turning simultaneously. Smolnik and Lücke [11] also describes these observations and indicates that this speed difference adds a new level of complexity.

A new harvesting process begins as soon as the machines finish turning and are at the beginning of a new lane. Again, the machines drive closely and nearly at the same speed to harvest and overload forage.

Furthermore, another TM can sometimes be close to the FH. For example, an empty TM that waits to work with the FH in the next platoon drives close behind the current platoon at the same speed to be ready in the vicinity.

Based on the above observations, I developed an algorithm for detecting plaitoing scenarios in the recorded harvest process data.

It starts by searching for every TM that could be in a harvest and overloading scenario with the FH by filtering the data points by the distance and speed difference between TM and FH. If the distance is less than 10 m, the speed difference is less than 5 km/h (1.39 m/s) and the FH and TM drive at a speed within 5 km/h...14 km/h (1.39 m/s...3.89 m/s), the TM could be in a harvest and overloading scenario with the FH.

In some cases, this algorithm would also detect the waiting TM. To avoid this, I applied a weighted sum of distance and speed difference between TM and FH to detect the harvest and overloading scenario. The weights are $\frac{3}{5}$ and $\frac{2}{5}$ for the distance and speed difference, respectively, to ensure that the closer TM is more likely in a harvest and overloading scenario with the FH, when they are moving at nearly the same speed. I determined the weights using the Trial-and-Error method,

⁶<https://dash.plotly.com/introduction>

setting the weights and displaying the found platoons scenarios on the map. Then I adjusted the weights until the detected platoons scenarios appeared correct.

For verification purposes, I displayed the found platoons scenarios on the map and confirmed that the found platoon appeared correct and the weights were set correctly.

After the platoons scenarios were correctly detected, I included the data points before each harvest and overloading scenario till a maximum distance of 50 m between FH and TM was exceeded. These data points are also relevant to the requirements because at the beginning of an agricultural platooning service, the FH, as the system leader, must be able to guide an empty TM to the appropriate position for overloading. Furthermore, no turning manoeuvres are detected. So far, the algorithm only detected consecutive time intervals, where the TM and FH are in a harvest and overloading scenario driving down the field. By adding the data points until a distance of 50 m before every time interval, the turning manoeuvres with their turning radii are also included in the detected harvest and overloading scenarios.

The final output shows the detected harvest and overloading scenarios with the FH and TM, which have roughly the same length every time the FH and TM are in a harvest and overloading scenario. This verifies that the algorithm is operating correctly, as it should generally take roughly the same time to fill the constant volume of TM's trailer with forage.

I also implemented the following verification method to determine whether the found platoon scenarios were correct. I observed that a fully loaded TM leaves the field via one of the field exits to bring the crop to a farm building. Via a check, if it has left the field and thereby passed the exit after leaving a platoon, wrongly recognised platoons can be detected.

The data points of a detected harvest and overloading scenario are represented in Figure 3.1. The FH and TM, plotted as black and white lines respectively, drive from the left lower corner to the top middle of the map in 3.1a. In between, the FH and TM do 2 turning manoeuvres on the right side of the map in 3.1a. At the end of the scenario, the TM turns to the right and heads towards the field exit.

The plotted distance and velocity data in 3.1b illustrates the same events. In the beginning, the TM drives with a higher velocity to catch up with the FH's position. After that, the TM and FH drive with a similar velocity and a distance below 10 m down the field lane. As soon as a turning manoeuvre starts, the distance increases and the velocity difference can be seen. After every turning manoeuvre, the TM and FH drive again with a similar velocity and a distance below 10 m. In the end, when the TM is full and leaves the harvest and overloading scenario, the distance increases and the TM drives at a higher velocity.

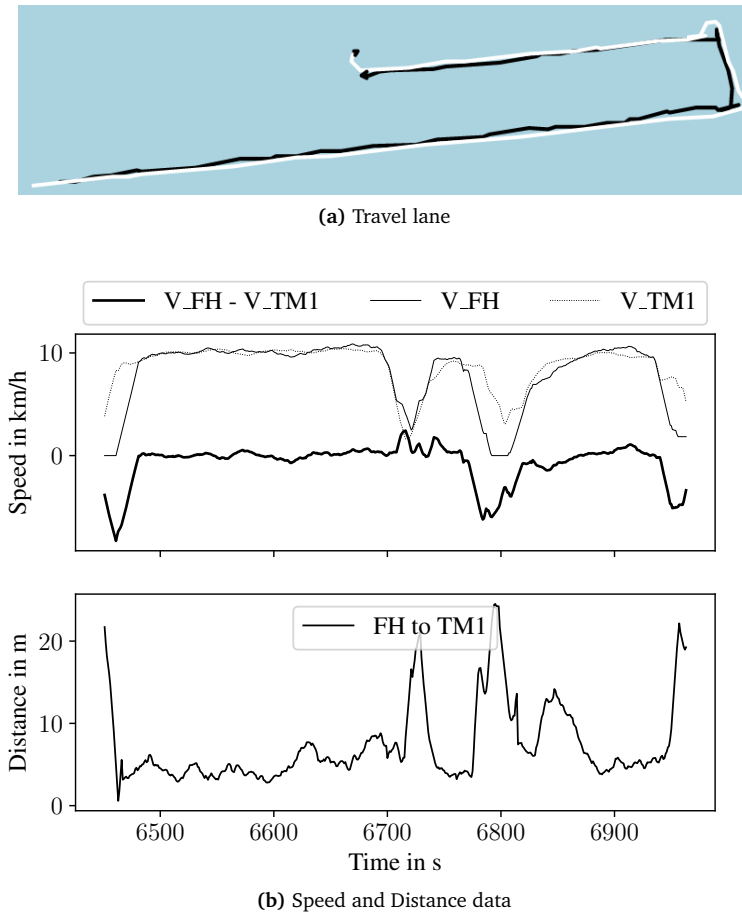


Figure 3.1 – A FH and a TM in harvest and overloading scenario, which is represented as distance and speed data plotted in regards to the time and which is visualised as a black and white travel lane for the FH, TM respectively

For the detected data points of the platooning services from recorded data of the corn harvest, the proportion where the FH and TM move in a specific distance is shown in Figure 3.2. For the same data points, the proportion in which FH and TM move at a given speed is available in Figure 3.3.

These results show that the TM and the FH usually move with a distance of less than 10 m. In addition, the distance can also be higher, e.g. in turning manoeuvres or before the overloading process.

Smolnik and Lücke [11] specifies the required communication range of platooning services in the corn harvest process as less than 30 m.

One notable observation in Figure 3.3 is that the FH and TMs in the corn harvesting platooning scenario often travel at a speed of approximately 10 km/h. This speed is significantly higher than the average speed of 6.6 km/h...8.1 km/h (1.9 m/s...2.2 m/s) of a FH operating on a 80 ha field from [7]. Nedelcu et al. [53]

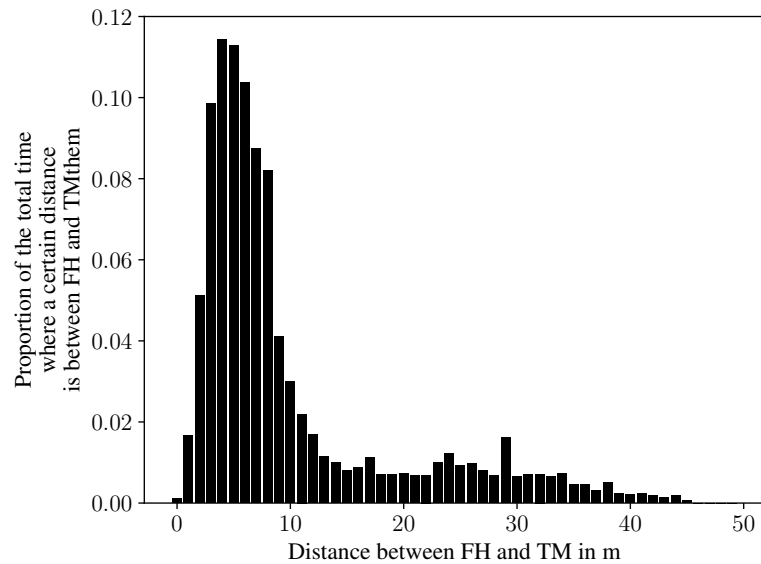


Figure 3.2 – Distribution of time proportions where a given distance was between Forage Harvester (FH) and Transport Machine (TM) in a harvest platoon scenario.

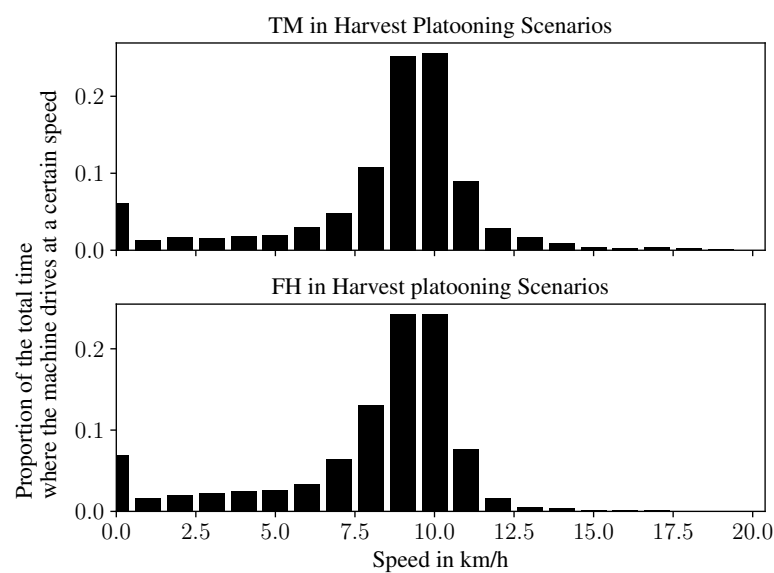


Figure 3.3 – Distribution of time proportions where Forage Harvester (FH) and Transport Machine (TM) drove with a certain speed in a harvest platoon scenario

report a optimal working speed of 2.6 km/h... 6.3 km/h (0.73 m/s... 1.75 m/s) for a FH which depends on the PD.

It is necessary to classify that in the year of the recorded data was little precipitation, so the corn was not dense and high, and the FH could drive faster. Nevertheless, the recorded data shows that a platooning service in agriculture must also be designed for higher speeds.

In Figure 3.3 is a local maximum at a speed of 0 km/h. In a harvest platoon scenario, FH and TM can stand still briefly when the cutting device is jammed. The driver's specific actuation usually clears the forage jam of the cutting device so that the platoon can continue its work.

Smolnik and Lücke [11] defines an average speed of 4.5 km/h for the development of platooning services in the corn harvesting process. Depending on the PD, the speed can vary from 2 km/h... 6 km/h according to the authors. The authors do not give a basis for the figures. However, the report is from the agricultural machinery manufacturer CLAAS, which is a major producer of FH worldwide and thus can be regarded as having good knowledge of the topic.

Klingler, Blobel, and Dressler [43] investigated the suitability of IEEE 802.11p for WIC. The authors detected that shadowing effects occur in the harvest scenario. The authors explain the effect because the spout of the FH was in LOS. I reviewed the recorded position data to get an overview of the TM's position relative to the FH in the overloading process. The relative bearing is the angle between the position of the TM and the heading of the position of the FH. Using the previous position of the FH, the relative bearing between FH and TM can be calculated with the angles α and β in Figure 3.4 as:

$$\text{Relative Bearing} = \beta - \alpha, \quad (3.1)$$

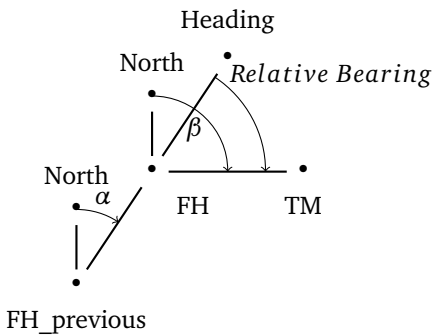


Figure 3.4 – Relative bearing between FH and TM which is calculated using the previous location of FH by using β and α for Equation 3.1

Assuming that the FH does not move backwards, the relative bearing describes the relative angle from the FH to TM. The result is displayed in Figure 3.5. It can be observed that the TM is mainly close to the FH at an angle of $30^\circ \dots 150^\circ$ at a distance between $0 \text{ m} \dots 10 \text{ m}$.

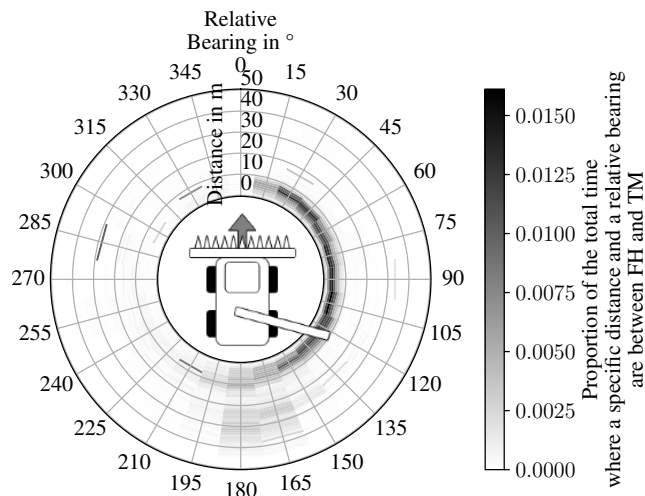


Figure 3.5 – Distribution of time proportion at specific distances and relative bearings between Forage Harvester (FH) and Transport Machine (TM)

In addition, it is noticeable that the machine can also be directly behind the FH. This driving behind each other is typical when a new part of the field is being cut in harvesting, as shown in Figure 3.6. When there is a greater distance between TM and FH, the TM is usually behind the FH at an angle of $157.5^\circ \dots 187.5^\circ$. At these moments, the TM is empty and closes up to the FH to operate in a new plaitoing Service together.



Figure 3.6 – Forage Harvester (FH) and Transport Machine (TM) start cutting a new field section

Another notable fact is that the TM hardly ever stayed to the left of the FH. Since the FH often made left turns, the crop was usually already harvested to the right of the FH so that the TM could drive there without running over the crop. On rare occasions, the TM was also to the left of the FH. Such a platooning scenario can be an exception or a driving manoeuvre to start cutting a new part of the field.

The results reveal only a first impression of the requirements of the harvest and loading process. More data from around the world must be analysed to make a general statement. The low rainfall this year resulted in a low plant population. This field condition made a higher process speed possible. The data may also vary based on the size of the agricultural machinery. Using a smaller FH would result in a smaller distance between TM and FH. To make a general statement, I should use data from different years, machines or harvest and loading scenarios because they can reveal other initial field conditions.

Einordnen in andere Scenarios

Chapter 4

Field Measurements

Figure 3.4 shows that the TM can be positioned at various distances and angles in relation to the FH. For one corn harvest scenario, Klingler, Blobel, and Dressler [43] found out that the RSS can drop due to shadowing effects caused by the size and shape of the FH and the TM.

In a field experiment, I want to analyze which positions of the TM and FH cause the shadowing effects which subsequently reduce the RSS, and how physical layer parameters like MCS and STBC can be used to ensure a low PER.

For the experiment, I will use a Combine Harvester (CH) instead of a FH as it has a similar shape and size as a FH and is available. The TM will be a Tractor pulling a trailer of the type HW80. Both machines will be equipped with a Global Positioning System (GPS) receiver and Wi-Fi devices which record the position, RSS and the PER of the exchanged packets. The CH will be positioned in an agricultural field. The tractor will start 50 m behind the CH, advance to the CH and pass the CH slowly with a speed of 1 km/h...5 km/h (0.28 m/s...1.39 m/s) as shown in Figure 4.1. While driving along the specified path, the tractor will mimic various overloading positions, where shadowing effects can occur. After the tractor has passed the CH, it will drive back to its starting position, and the experiment will be repeated with different overloading distances between the CH and the tractor.

During the experiments, GPS receivers at the agricultural machines will record the position and speed of the machines every 1 s.

The Wi-Fi setup consists of a Milesight Industrial Router UR75⁷, which implements the standards IEEE 802.11 b/g/n in the 2.4 GHz band and IEEE 802.11 a/n/ac in the 5 GHz band and IEEE 802.11 a/n/ac in the 5 GHz band. The router is equipped with two omnidirectional antennas for 2.4 GHz and 5 GHz usage. Brinkhoff and Hornbuckle [47] and Paul et al. [52] already found out that placing the antenna

⁷<https://iot-shop.de/en/shop/mil-ur75-500gl-g-p-w-milesight-ur75-500gl-g-p-w-industrial-cellular-5g-router-with-gps-wifi-and-poe-5677>

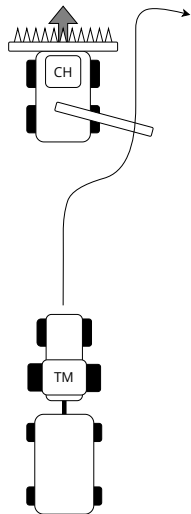


Figure 4.1 – Path around the static Combine Harvester (CH), which the Transport Machine (TM) will drive during the experiment to mimic various overloading positions

higher above ground improves the robustness and communication range of Wi-Fi networks in an outdoor environment. As the regulation in the German Law StVZO §32 Abs. 2 limits the height of every agricultural vehicle or combination of vehicles to less than 4.0 m, the maximum antenna height is 4 m above the ground. Therefore, I will mount the router on the tractor's roof at a height 4 m above the ground.

I set up two Wi-Fi devices on the CH, which are two UP Squared Boards⁸ with an Intel AX210 Wi-Fi module⁹.

Every Intel AX210 Wi-Fi module supports the IEEE 802.11ax standard for 2.4 GHz, 5 GHz and 6 GHz band and is equipped with two antennas, which support omnidirectional transmissions in the 2.4 GHz, 5 GHz and 6 GHz band and have a gain of 5 dB. The boards are mounted on the roof of the CH next to one another at a height 4 m above the ground too.

The router on the tractor sets up a Wi-Fi AP. One of the boards on the CH connects to the AP of the router as a Wi-Fi STA and hosts an iperf3¹⁰ server. A notebook is connected via LAN to the router and runs an iperf3 client, which connects to the iperf3 server on the CH. The iperf3 client sends 100 Byte UDP packets every 100 ms to the iperf3 server on the CH. The server records the received packets.

Many different Wi-Fi transmissions arise through the iperf3 UDP packets, the Wi-Fi manager of the Milesight Industrial Router, and the Intel AX210 Wi-Fi card. These transmissions can be RTS/CTS, ACK, Data, Beacon or Probe request frame,

⁸https://eu.mouser.com/datasheet/2/826/UP_Square_DatasheetV0_4-3084829.pdf

⁹https://docs.alfa.com.tw/datasheets/alfa-network_ait-ax210-ex_latest.pdf

¹⁰<https://iperf.fr/>

displayed in Figure 4.2. Through testing, I found out that the Wi-Fi manager of the Wi-Fi devices can apply VHT MCS 0…9 and STBC as physical layer configurations.

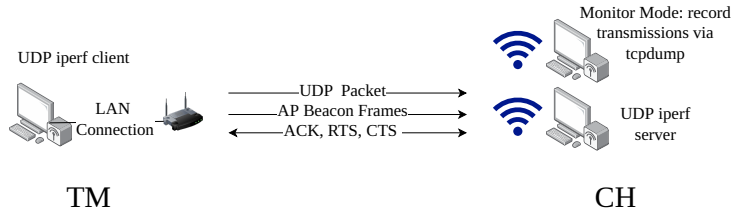


Figure 4.2 – Wi-Fi transmissions between the Wi-Fi AP on the Transport Machine (TM) and the Wi-Fi STA on the Combine Harvester (CH), which are recorded by a third Wi-Fi device in monitor mode on the CH

The other UP Squared Board on the CH uses the Wi-Fi card in the monitor mode and records every transmission in the 5.6 GHz band using `tcpdump`¹¹. Since the UP Squared board is placed next to the other board on the roof of the CH, it can record the same signals the other board receives in the UDP transmission. The `tcpdump` records are in pcap - format, which can be analyzed using Wireshark¹². Using Wireshark, my plan is to identify possible retransmissions to calculate a PER. At the same time, the data contains the RSS of each antenna and the physical layer parameters for every transmission, allowing each transmission's robustness to be calculated as a function of the RSS and the physical layer configuration.

In order to get insights on the robustness of using the different frequency bands, the frequency channels for a BW of 20 MHz in Table 4.1 are configured. To be able to calculate the means and standard deviations of the result for every configuration, the experiment is repeated 5 times for each channel, which means that the tractor drives 5 times the same path, which is displayed in Figure 4.1.

BW	Channel number 2.4 GHz	Channel number 5 GHz
20 MHz	1	100
40 MHz	3	102
80 MHz	-	106

Table 4.1 – Frequency channel numbers for 2.4 GHz and 5 GHz for the different Bandwidth (BW)s of the IEEE 802.11 standard [16], which can be used for outdoor communication [54], [55] and can be configured in the Milesight Industrial Router UR75 for the field experiments.

¹¹<https://www.tcpdump.org/>

¹²<https://www.wireshark.org/>

4.1 Trial Run

Since it rained a lot before the planned field experiments, I did a trial run to ensure that the experiment worked as expected and I got the data I needed. I mounted the Wi-Fi devices on the TM and the CH as shown in Figure 4.3 and started the iperf3 client and server on the CH and the TM respectively. During the trial run, the machines kept the same positions in a yard at the university. To vary the recorded RSS, I simultaneously moved the Wi-Fi antennas of the Wi-Fi devices on the CH to different positions. I varied the BW between 20 MHz...80 MHz in reference to Table 4.1. The trial run was partly successful. The monitoring Wi-Fi device blocked any try to configure monitoring channels with higher BWs than 20 MHz. Therefore, I could only record data for a BW of 20 MHz.

The recorded data contains RSS, physical layer configuration and MAC layer information of every received packet. This can be used to find shadowing and fading effects, which may occur in the corn harvest scenario.

The recorded data was filtered to contain only the UDP packets sent by the iperf3 client on the TM and displayed in Figure 4.4. It is visible that the Wi-Fi rate manager on the Milesight Industrial Router UR75 does not use STBC and varies the MCS between 5...8 and the GI between 400 ns...800 ns. Due to moving the antennas, the RSS varies until I placed the antennas at a suitable fixed position at the end of the trial run. As soon as the RSS drops significantly at around 25 s...50 s, the Wi-Fi rate manager switches to a lower MCS and a longer GI to increase the transmission's robustness and reduce the retransmissions, which are indicated by the retry flag in the UDP packet.

The trial run took place in a yard at the university, where shadowing and fading effects due to buildings, trees, and agricultural machines are expected. The university ran other Wi-Fi networks, which may have interfered with my Wi-Fi network. Therefore, many packets can get lost due to interference, shadowing or fading.

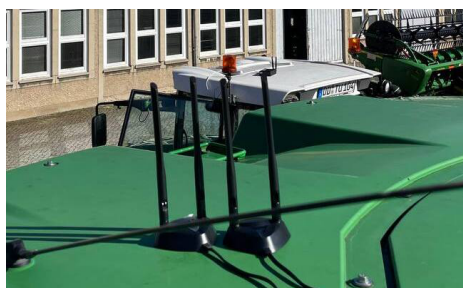


Figure 4.3 – Position of the Wi-Fi Devices on the TM and the CH during the trialrun

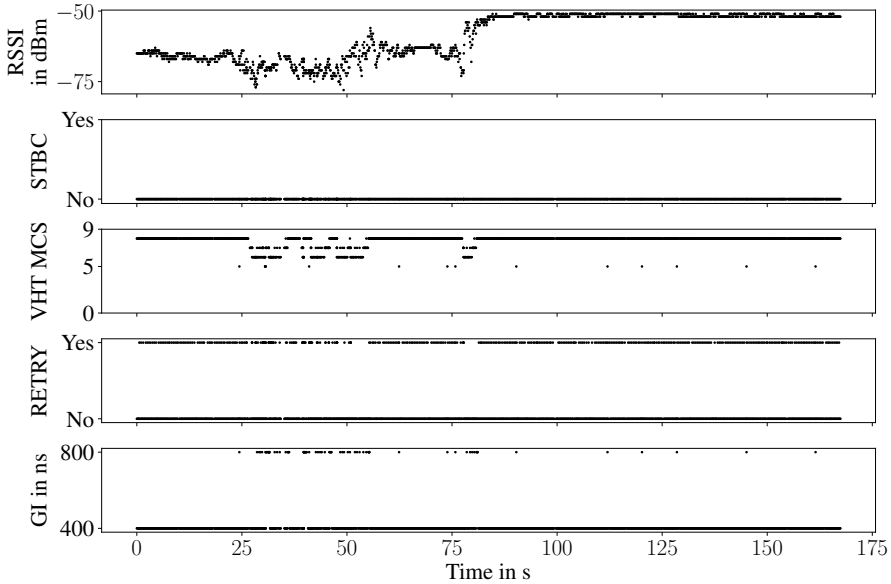


Figure 4.4 – All QoS data transmissions between the Wi-Fi Access Point (AP) on the Transport Machine (TM) and the Wi-Fi STA on the Combine Harvester (CH) in a trial run, which were initiated by the iperf3 client on the Transport Machine (TM)

Every UDP packet contains a sequence number to identify the packet. If the packet is a retransmission, the packet contains the retry flag with the same sequence number and data of the original transmission. In general, 25 % of received UDP data packets contained retry flags. This cannot be transferred to the PER directly, as it is unknown how many transmissions were sent by the iperf3 client and were lost due to interference, shadowing or fading. To calculate the PER, an additional Wi-Fi monitoring device next to the Wi-Fi router on the TM is needed to record all outgoing transmissions of the iperf3 client. The PER can then be calculated as the ratio of every successfully received UDP packet to the number of transmitted UDP packets.

Alternatively, retransmissions could be disabled as Klingler, Blobel, and Dressler [43] did in their experiments. Then every packet, which is missing in the sequence of received packets, is counted as a lost packet. But the user interface of the Milesight Industrial Router UR75 has no option to disable retransmissions.

It is notable that the Wi-Fi rate manager on the Milesight Industrial Router UR75 always tries to use two spatial streams, the highest MCS and the shortest GI possible, which results in the highest theoretical data rate. For the BW of 20 MHz, the highest MCS is 8 and the shortest GI is 400 ns [15]. This translates to a theoretical data rate of 173.3 Mbit/s, which is overdimensioned for the UDP data packet rate of 100 Byte

every 100 ms. Additionally, the communication is less robust, which results in the high percentage of 25 % of known retransmissions.

In the end, I could not conduct the proposed field experiments due to the rainy weather, which led to very wet agricultural fields.

4.2 Wi-Fi Range Measurements

Instead, I conducted a range measurement in an outdoor environment on an abandoned airfield near Mahlwinkel ($52^{\circ}23'17.9''\text{N}$ $11^{\circ}50'35.4''\text{E}$) in Saxony-Anhalt, Germany, which can be seen in Figure 4.5. The airfield was surrounded by grassland, wind turbines, a solar park and forests, which describe a typical environment for agricultural machines.



Figure 4.5 – Airfield near Mahlwinkel ($52^{\circ}23'17.9''\text{N}$ $11^{\circ}50'35.4''\text{E}$) in Saxony-Anhalt, Germany, where I conducted the range measurements

I set up the Wi-Fi devices according to the setup above, where I replaced the CH with a 4 m wooden antenna mast and the TM with a roof extension on top of a car rack to reach a height of 4 m. The setup is shown in Figure 4.6.

The two Wi-Fi devices are mounted on the wooden antenna mast and were configured to run the iperf3 server and the monitoring mode. I connected a GPS receiver to the monitoring device and recorded the static position of the wooden antenna mast. The wooden extension on top of the car rack carried the Wi-Fi router with the iperf3 client and an GPS receiver to record the car's position every second.

I place the Wi-Fi devices on the wooden antenna mast at one end of the airfield ($52^{\circ}23'17.8''\text{N}$ $11^{\circ}50'41.7''\text{E}$) and drove the car with a speed of around 10 km/h (2.78 km/h) the other end of the airfield ($52^{\circ}23'17.8''\text{N}$ $11^{\circ}50'29.7''\text{E}$). Meanwhile, the iperf3 application exchanged 100 Byte UDP packets every 100 ms. Every Wi-Fi transmission, which was received by the monitoring device, was recorded. The iperf3 application ran while I drove away and back to the starting point. I repeated this procedure three times to get a reliable result.



Figure 4.6 – Setup of the Wi-Fi devices for the range measurements, which I mounted on wooden antenna masts to reach a height of 4 m, the maximum allowed height of agricultural machines in Germany

As I started the iperf3 client after the monitoring device, the first UDP packets were recorded and used as a time reference to synchronize the GPS data of the car and the monitoring device. I also used the recorded GPS time stamps to synchronize the recorded Wi-Fi transmissions with the GPS logs.

The range measurement results are shown in Figure 4.7. I received Wi-Fi transmissions up to a distance of 2.5 km, which equals the length of the airfield.

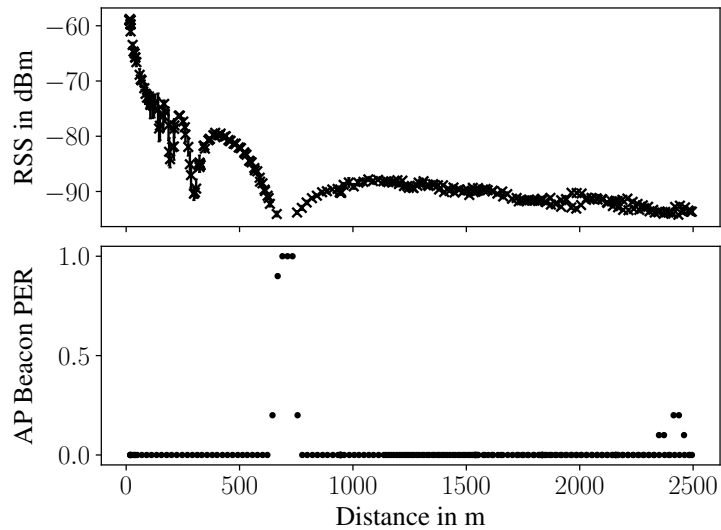


Figure 4.7 – Range measurement results of the Wi-Fi transmissions on the airfield near Mahlwinkel ($52^{\circ}23'17.9''N$ $11^{\circ}50'35.4''E$) in Saxony-Anhalt, Germany

The RSS values reflect a typical two-ray ground reflection model, where the ground reflection can be seen as a second ray, which can cause destructive interference with the direct ray. The destructive interference can be seen as the drops in the RSS values.

At a distance of around 650 m ... 750 m, the RSS values drop below the sensitivity of the Wi-Fi devices and no Wi-Fi transmissions are received anymore.

This effect can also be detected in the PER values of beacon frames. The Milesight Industrial Router UR75 broadcasts every 100 ms the AP beacon frame, which is used by Wi-Fi devices to authenticate and associate with the AP. This beacon frame interval is defined in the recorded beacon frames and allows me to calculate the PER of the beacon frames as every s 10 beacon frames should be received by the monitoring device. The PER of the beacon frames is shown in Figure 4.7 and indicates that no beacon frame was received at a distance of around 650 m ... 750 m, because the RSS values dropped below the sensitivity of the Wi-Fi devices.

Every beacon frame is transmitted in the IEEE 802.11a standard with a data rate of 6 Mbit/s, which can also be received by older Wi-Fi devices. A data rate of 6 Mbit/s refers to Binary PSK modulation with a CR of 1/2 [56]. This MCS and CR combination is the most robust combination, which caused the low PER values of the beacon frames over the large communication range of up to 2.5 km. However, at the end of the communication range, the PER values of the beacon frames started to increase, because the RSS values suffer more from multipath, shadowing and fading effects and are not high enough to be sensed by the Wi-Fi devices.

to discuss, sehr weit aus dem Fenster gelehnt. Ich vermute

4.3 Field Measurements Evaluation

The achieved Wi-Fi transmission range may be dependent on the antenna height. Brinkhoff and Hornbuckle [47] concluded that the antenna height has a significant impact on the Wi-Fi transmission range. They state, that the Wi-Fi transmission range increases with the antenna height, because the Wi-Fi transmissions are less affected by obstacles and the Fresnel zone is less obstructed. This effect is available until a maximum antenna height of 50 m by the authors.

In regard to antenna height, future field experiments should be conducted to find the optimal antenna height for agricultural machines. Antennas heights can be built retractable and extendable to stay below the maximum allowed height of 4 m for agricultural machines in Germany on public roads and to be able to extend the antenna height to the optimal height for the Wi-Fi transmission range in agricultural fields.

Ground reflection coefficient beton grass, permeability, conductance, permittivity of grass, permittivity of concrete, permittivity of air, permittivity of water

WIC uses cases require reliable communication between the agricultural machines to exchange data with each use case's specific required data rate, range, and latency.

The range measurements indicate that the Wi-Fi transmissions can be received up to a distance of 2.5 km, which is sufficient to cover substantial agricultural fields. However, Wi-Fi transmissions suffer from multipath, shadowing and fading effects, which can cause a large number of retransmissions, when the physical layer configuration is oriented towards a high data rate instead of high robustness as it was in the trial run.

As every used Wi-Fi device in the field experiment runs a Wi-Fi rate manager, which is responsible for the rate adaptation, the influence of a particular physical layer parameter on the data goodput, robustness and latency can not be examined in the field experiment as no particular physical layer parameter can be set. The Milesight Router is only capable of setting IEEE 802.11ac physical layer parameters, which don't include the new physical layer parameters of IEEE 802.11ax: ER mode, longer GIs, HE-MCS 9...11 or DCM.

Taking DCM as an example, the impact on the Wi-Fi receiver minimum input level sensitivity was mentioned in Figure 2.4. DCM increases the robustness of the Wi-Fi transmissions and therefore allows a lower receiver minimum input level sensitivity to be used.

In the following chapter, I will analyze in simulations which physical layer configurations are suitable for the agricultural environment to establish reliable communications, which meets the data rate, range and latency requirements of Agricultural Platooning Services.

Chapter 5

Link Level Simulation

Simulations benefit from the flexibility and possibility of simulating different communication and network protocols [57].

Simulations are considered the main evaluation method for IEEE 802.11ax networks by the IEEE 802.11ax task group [29].

The authors distinguish between link-level and system-level simulations for simulating HE wireless networks. The authors explain both methods as follows.

For system-level simulation, it requires abstractions of the physical and MAC layers to simulate a system close to real on this basis.

Link-level simulations, according to the authors, investigate the performance of the HE physical layer for different physical layer parameters as PER in terms of SNR. As an example, the authors cite multiple different researchers, which simulated PER regarding SNR and chosen MCS. Link-level simulations are usually visualised in so-called waterfall plots, which represent the PER regarding SNR for different physical layer parameters.

5.1 Robustness

The following section analyzes the impact of the different physical layer parameters of the IEEE 802.11ax standard on transmission robustness in a Link-Level Simulation.

A known simulation tool for wireless communication networks is GNU Radio¹³. GNU Radio is an open-source software development toolkit with additional blocks for IEEE 802.11 network simulation, called gr-ieee802-11¹⁴. However, the gr-ieee802-11 only supports the IEEE 802.11a, IEEE 802.11b, IEEE 802.11g and IEEE 802.11p. This means that the gr-ieee802-11 does not support the ER mode, DCM or STBC. Therefore, I decided that GNU Radio was not suitable for my simulation.

¹³<https://www.gnuradio.org/>

¹⁴<https://github.com/bastibl/gr-ieee802-11>

Sheela, Kuri, and Akhtar [58] cites ns-3¹⁵ to mention that ns-3 does not implement any frequency-selective fading effects, such as multipath propagation and shadowing. Therefore, the authors decided to use the MATLAB WLAN Toolbox, which is standards-compliant and credible. I also decided to use Matlab because besides [58], [59] and [60] have also considered the MATLAB WLAN Toolbox to be suitable for IEEE 802.11ax simulations.

The MATLAB WLAN Toolbox¹⁶ is an add-on to simulate, analyze, and test wireless LAN communication systems. The WLAN Toolbox supports a wide range of IEEE 802.11 standards. Since Release R2019b¹⁷, the WLAN Toolbox supports the Signal Recovery, Packet Extension and Physical Layer abstractions to simulate IEEE 802.11ax networks.

My robustness analysis is based on the WLAN Toolbox example wlan/HESUExample¹⁸ to simulate the PER of point-to-point IEEE 802.11ax networks for specified SNR values.

First, I set the IEEE 802.11ax physical layer parameters using the wlanHEConfig object, where I define the default settings in Table 5.1.

Next, I chose a channel model to simulate the channel. The WLAN Toolbox supports a wide range of channel models, such as wlanTGaxChannel, wlanTGN-Channel, wlanTGacChannel, and wlanTGNChannel. The TGax channel models are MIMO broadband channel models for IEEE 802.11ax networks, which include spatial channel models, doppler effects, path loss, building penetration loss and shadowing effects [61]. The wlanTGaxChannel model supports 6 different sub-channel models, named TGax-A, TGax-B, TGax-C, TGax-D, TGax-E, and TGax-F, where the TGax-F

¹⁵<https://www.nsnam.org/docs/models/html/wifi-design.html>

¹⁶https://de.mathworks.com/products/wlan.html?s_tid=A0_PR_info

¹⁷<https://de.mathworks.com/help/wlan/release-notes.html>

¹⁸<https://de.mathworks.com/help/wlan/ug/802-11ax-packet-error-rate-simulation-for-single-user-format.html>

Parameter	Chosen Default Settings
GI	3200 ns
BW	20 MHz
Number Spatial Streams	2
Number Transmit Antenna	2
DCM	disabled
STBC	disabled
HE-MCS	0
ER	disabled
LDPC	enabled

Table 5.1 – Default physical layer settings for the IEEE 802.11ax robustness simulations

channel model is suitable for pseudo-outdoor scenarios [61]. The TGax channel models were used for Matlab Wlan Toolbox simulations by [58], [59] and [60].

[61] and [29] list that the IEEE 802.11ax task group has also implemented the channel models UMa and UMi for outdoor urban scenarios. However, the WLAN Toolbox does not support these channel models, and they are intended for urban scenarios.

As I want to simulate outdoor scenarios, I chose the most appropriate channel model TGax-F, which is suitable for pseudo-outdoor scenarios [61]. The wlanTGax-Channel model supports configuring the BW, the number of transmit and receive antennas, which I set equal to the configuration of the wlanHEConfig object. [54] and [55] allow outdoor transmission in the frequency range of 5.725 GHz to 5.825 GHz. Therefore, I set the carrier frequency to 5.6 GHz. The TGax-F channel sampling rate is set to 20 MHz, which is the nominal sampling rate for the configured BW of 20 MHz. Additional parameters are left at their default values as they are irrelevant for outdoor scenarios. According to the MATLAB WLAN Toolbox documentation ¹⁹, the TGax-F channel model has a maximum multipath propagation delay of 1050 ns and root mean square delay spread of 150 ns.

The simulations are based on Algorithm 5.1. To get a PER for every SNR value ranging 0 dB ... 45 dB, the Algorithm 5.1 is executed 5 times for 500 packets each. All packet errors are counted, and the PER is calculated by dividing the number of packet errors by 500 packets. A mean PER and the confidence interval with a confidence level of 95 % is calculated of the PER values of the 5 iterations.

¹⁹<https://de.mathworks.com/help/wlan/ref/wlantgaxchannel-system-object.html>

Require: Global variable *numPacketErrors*

- 1: Create random packet data *txData* of length 1000 Byte
 - 2: Create transmission waveform *txWaveform* from packet data *txData*
 - 3: $rxWaveform \leftarrow txWaveform$ passed through TGax channel model
 - 4: Add noise to *rxWaveform* based on SNR value
 - 5: Run packet detection on *rxWaveform*
 - 6: **if** no packet detected **then**
 - 7: $numPacketErrors \leftarrow numPacketErrors + 1$
 - 8: **end if**
 - 9: Detect packet delay *delay*
 - 10: **if** *delay* > 50 samples **then**
 - 11: $numPacketErrors \leftarrow numPacketErrors + 1$
 - 12: **end if**
 - 13: Steps to recover packet data *rxData* from *rxWaveform*
 - 14: **if** *txData* != *rxData* **then**
 - 15: $numPacketErrors \leftarrow numPacketErrors + 1$
 - 16: **end if**=0
-

Algorithm 5.1 – Procedure to detect packet errors

The Algorithm 5.1 starts with the creation of a random packet of the specified length of 1000 Byte. The packet is used to create a Wlan waveform based on the physical layer parameters specified in the wlanHEConfig object using the wlanWaveformGenerator function.

The waveform is extended by 50 trailing zeros to ensure that packet delays can be detected by finding trailing samples unequal to null. Since the possible maximum detectable channel delay can be calculated by

$$\text{detectable channel delay} = \frac{\text{length of trailing zeros}}{\text{Sampling rate}}, \quad (5.1)$$

then 50 trailing zeros match a maximum channel delay of 2.5 μs . As the maximum channel delay of the TGax-F channel model is 1.05 μs , 50 trailing zeros are sufficient to detect the maximum channel delay. I verified Equation 5.1 by comparing the length of the maximum detected packet delay with the maximum channel delay of the TGax-F channel model. The results showed that the maximum seen packet delay is 11 samples, which can be transferred using Equation 5.1 to rounded maximum TGax-F channel delay of 1.1 μs .

After creating the waveform and appending the trailing zeros, the waveform is passed through the TGaxF channel model to simulate the channel. The output of the channel model is the received waveform, where I added noise to the received waveform based on the specified SNR value and active OFDM subcarriers.

In the next step, the received waveform is passed through the packet detection algorithm, which is based on the WLAN Toolbox example wlan/HESUExample²⁰ and shown in an abstracted form in Algorithm 5.1. The procedure calls various functions to decode the preamble, header and payload of the received waveform. A packet error is detected when no packet arrives, the packet delay is greater than 50 samples or the recovered packet data is not equal to the transmitted packet data.

Modulation and Coding Scheme (MCS) and Coding Rate (CR)

In the first simulation run, I analyzed the influence of a chosen set of HE-MCS values on the PER regarding the SNR. The results in Figure 5.1 show that the PER decreases with higher SNR for all HE-MCS values. The PER decreases at lower SNR values for lower HE-MCS values. Increasing the HE-MCS value by 2 increases the SNR, where a PER of less than 10 % is achieved, by 5 dB ... 6 dB.

²⁰<https://de.mathworks.com/help/wlan/ug/802-11ax-packet-error-rate-simulation-for-single-user-format.html>

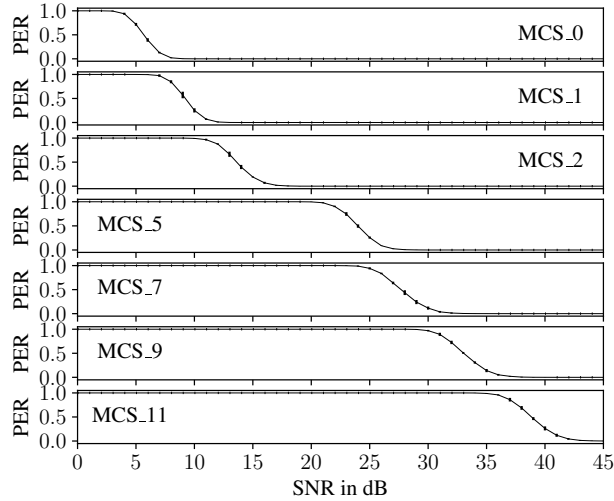


Figure 5.1 – Simulated PER regarding SNR for chosen HE-MCS values for IEEE 802.11ax physical layer parameters of a GI of 3200 ns, a bandwidth of 20 MHz and 2 spatial streams.

Paul et al. [52] conducted outdoor experiments to analyse the error rate and SNR of different IEEE 802.11n MCS for the communication distances of 300 m, 800 m and 1800 m. Their results show that SNR decreases when the transmissions range is longer. Additionally, they experienced a higher error rate for higher MCSs.

The effect that the PER decreases when a lower MCS or CR is used is the basis for the design of Wi-Fi rate managers. A rate manager is a software component that selects physical layer parameters, such as MCS or CR, based on the current network conditions to achieve the best possible throughput. Known rate managers of the Linux kernel are the minstrel or the minstrel HT rate manager.

Forward Error Correction (FEC)

Another parameter that influences the PER is the forward error correction (FEC) procedure choice. To analyze the influence of the FEC procedure on the PER, I simulated the PER in regards to the SNR for HE-MCS 0...9 and whether LDPC or BCC is enabled. For higher HE-MCS values, BCC can not be used as LDPC is compulsory, so no comparison of the FEC procedures is possible.

The results are displayed in Figure 5.2. The PER decreases with higher SNR for both FEC procedures for all HE-MCS values as expected. Using LDPC instead of BCC, a PER of less than 10 % can be achieved at 2 dB lower SNR for all HE-MCS values. The effect increases to 3 dB with higher HE-MCS values than HE-MCS 5.

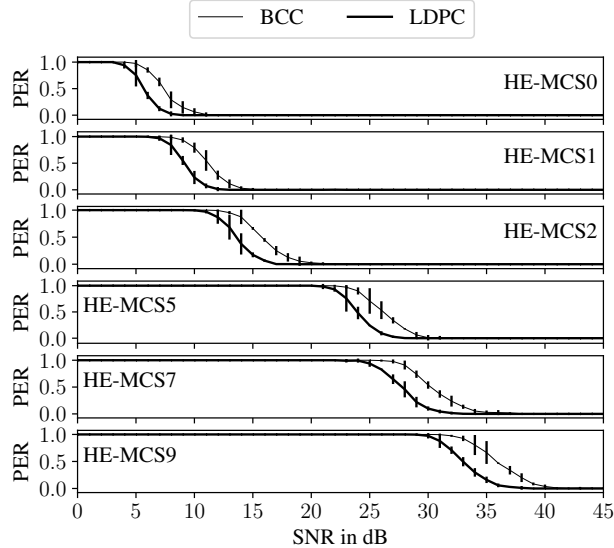


Figure 5.2 – Simulated PER in regards to SNR for chosen HE-MCS values and whether LDPC or BCC is enabled for IEEE 802.11ax physical layer parameters of a GI of 3200 ns, a bandwidth of 20 MHz and 2 spatial streams

Syafei et al. [20] simulated the effect of the FEC procedure on the PER for IEEE 802.11n. They had similar results and state that using LDPC instead of BCC, a PER of 0.1 % can be achieved at a 3.2 dB...6 dB lower SNR.

According to Tran et al. [62], this effect is also present for IEEE 802.11ac. A PER of 0.1 % can be achieved at a 1.1 dB lower SNR for using LDPC instead of BCC for 64 - QAM. The effect increases to 1.5 dB for 256 - QAM.

Guard Interval (GI)

Robustness against intercarrier and intersymbol interference can be achieved using a longer GI [22]. In order to analyse the impact of the GI on the PER, I simulated the PER regarding the SNR for different HE-MCS values and GIs. The results for a GI of 3200 ns and 800 ns are plotted in Figure 5.3. As expected, the PER decreases with higher SNR for all HE-MCS values. Using a GI of 3200 ns instead of 800 ns no significant difference of PER in regards to the SNR can be observed for HE-MCS values lower than 5. Increasing the HE-MCS value, the robustness of the MCS sinks and the effect of the intercarrier interference and intersymbol interference increases. As the maximum channel delay for the Tgax-F channel model is 1050 ns, the channel delay can be longer than the GI of 800 ns. This can result in intersymbol interference, which results in a higher PER for higher HE-MCS values. For HE-MCS5, a PER of less than 10 % can be achieved at 1 dB lower SNR for a GI of 3200 ns instead of 800 ns. The effect increases with higher HE-MCS values.

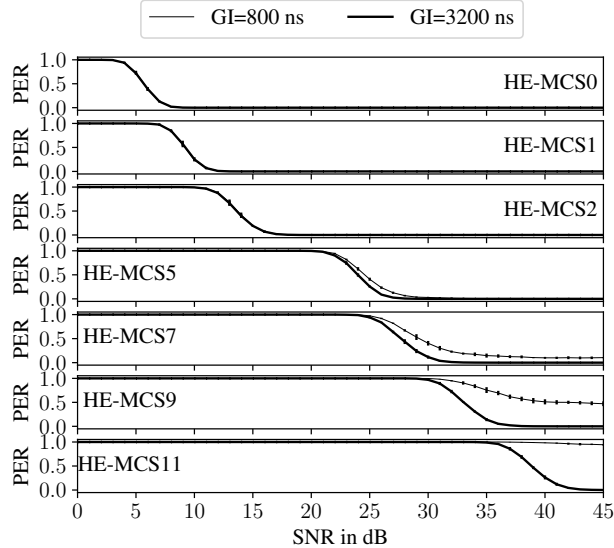


Figure 5.3 – Simulated PER in regards to SNR for chosen HE-MCS values and whether a GI of 800 ns or 3200 ns is enabled for IEEE 802.11ax physical layer parameters of a bandwidth of 20 MHz and 2 spatial streams

Patil et al. [63] conducted similar simulations for IEEE 802.11n. They agree that a longer GI can increase the robustness against longer delay spreads as they are in the TGn-E and TGn-F channel models, which are predecessors of the TGax-F channel model [61].

Dual Carrier Modulation (DCM)

Next, I simulated the PER in regards to the SNR and whether DCM is enabled for the specified HE-MCS values. I have used the possible HE-MCS 0,1,3 and 4 from the IEEE 802.11ax standard [16] for the simulation of DCM.

The results indicate that using DCM can achieve the same PER at lower SNR values compared to not using DCM. A PER of less than 10 % can be achieved at a 2 dB lower SNR when using DCM. The effect increases to 4 dB for HE-MCS values higher HE-MCS4. The results are plotted in Figure 5.4.

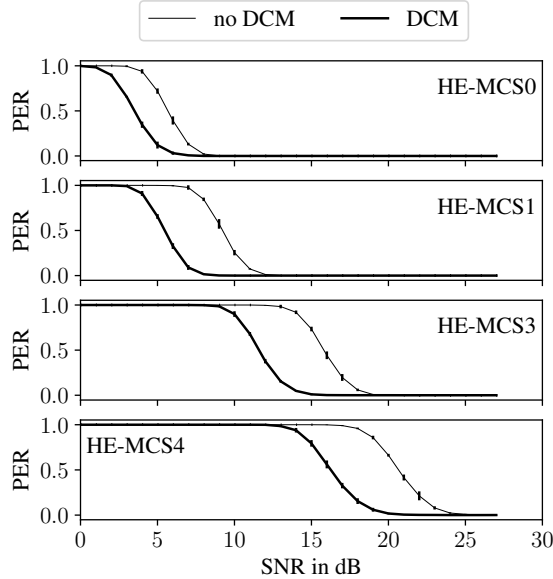


Figure 5.4 – Simulated PER in regards to SNR for chosen HE-MCS values and whether DCM is enabled for IEEE 802.11ax physical layer parameters of a GI of 3200 ns, a BW of 20 MHz and 2 spatial streams

Khorov, Kiryanov, and Lyakhov [64] also mention similar figures that DCM increases the PER performance by more than 2 dB.

Ryu, Lee, and Kang [65] and Park, Sung, and Ko [66] conducted a similar simulation, where they analyzed the bit error rate in regards to the normalized SNR and whether DCM was enabled for rayleigh fading channels. Both authors wrapped two Quadrature PSK modulated symbols into one 16-QAM symbol. As Quadrature PSK modulates 2 bit per symbol, the information of two Quadrature PSK modulated symbols can be transmitted in one 16-QAM symbol, which encodes 4 bit. The authors transmit the 16-QAM symbols and a redundant copy of the 16-QAM symbols via orthogonal subcarriers. At the receiver, the authors combine the copies and retrieve the transmitted information using the Maximum likelihood criterion. The results of the authors show that a better bit error rate can be achieved while applying DCM than sending the information via two Quadrature PSK or 16-QAM modulated symbols without DCM.

Extended Range (ER)

For a HE-MCS 0 and 1 the ER mode can be applied additional to DCM, when one spatial stream is used [16]. In order to analyze the impact of the ER mode, I set the physical layer parameters to a GI of 3200 ns, a BW of 20 MHz and one spatial

stream. For He-MCS 0, 1 and 3 I ran simulations, where I enabled the ER mode and compared the PER to the PER of the same HE-MCS values without ER mode.

The results in Figure 5.5 indicate that the PER is influenced by the ER mode. The difference in SNR with ER mode to without ER mode, where a PER of 10 % is achieved, is 1 dB...2 dB.

Additionally, I simulated the impact of applying the ER mode and DCM for the allowed HE-MCS values 0 and 1. Applying DCM additionally makes the transmission more robust. As it is displayed in Figure 5.5, a PER of less than 10 % can be achieved at a 4 dB...5 dB lower SNR when using DCM and ER mode together instead of using ER mode alone.

Jacob et al. [17] conducted a simulation, where they analysed the effect of DCM and ER on the PER for IEEE 802.11bd in vehicular environments to the transmission range. The authors found out that using DCM and ER can increase the transmission range for LOS by 65 % for a PER lower than 0.1. After additional analysis with higher vehicle densities, the authors remark that using DCM and the ER mode causes channel congestion in CSMA/CA based networks with low bandwidths. The authors conclude that the ER mode and DCM should be used for long-range transmissions, where the physical layer parameters can extend the transmission range significantly.

A similar simulation was conducted by Triwinarko, Dayoub, and Cherkaoui [28]. The researchers state that using DCM and the ER mode results in better PER performance at lower SNR values in LOS and non-LOS scenarios.

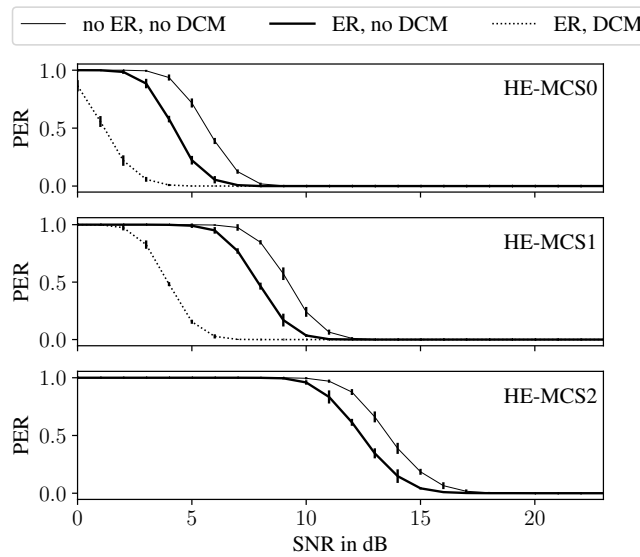


Figure 5.5 – Simulated PER in regards to SNR for chosen HE-MCS values and whether Extended Range or DCM is enabled for IEEE 802.11ax physical layer parameters of a GI of 3200 ns, a BW of 20 MHz and 2 spatial streams

Space-Time-Block-Code (STBC)

As aforementioned, additional robustness can be achieved by applying STBC. In order to analyse the impact of STBC on the PER in regards to the SNR, I run the simulation for the HE-MCS values 0 … 11 with and without STBC.

The results in Figure 5.6 indicate that the PER is influenced by the STBC mode. A PER of less than 10 % is possible at a 2 dB … 10 dB lower SNR when using STBC additionally. The impact of STBC on the PER grows from 2 dB for HE-MCS0 to 10 dB for HE-MCS11.

Stamoulis and Al-Dhahir [34] analysed the impact of STBC on the bit error rate for IEEE 802.11a in regards to the SNR. Their simulation was based on a HiperLAN/2 channel with 2 antennas. They used HiperLAN/2 because it has a physical layer similar to IEEE 802.11a. The authors found that applying STBC results in a lower bit error rate for a given SNR value. The authors conclude that STBC can be used to increase the robustness of the transmission.

Santumon and Sujatha [33] and Tarokh, Jafarkhani, and Calderbank [67] conducted simulations, where they analyzed the effect of STBC on the bit error rate for wireless communication systems. In general, the authors found out that STBC can be used to decrease the bit error rate for a given SNR value for different MCS values. Additionally, the authors remark that the impact of STBC on the bit error rate grows with the number of antennas. However, the number of antennas is limited to 2 for IEEE 802.11ax [16].

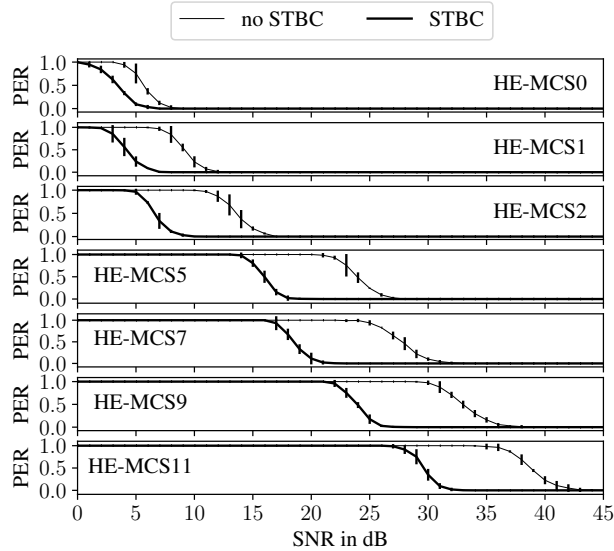


Figure 5.6 – Simulated PER in regards to SNR for chosen HE-MCS values and whether STBC is enabled for IEEE 802.11ax physical layer parameters of a GI of 3200 ns, a BW of 20 MHz and 2 spatial streams

2.4 GHz Frequency band

I conducted the same simulations for the frequency band of 2.4 GHz. Using the same physical layer parameters in the 2.4 GHz band achieve a similar PER in regards to the SNR and chosen physical layer parameters as in the 5 GHz band.

But how does the effect of the frequency bands on the PER in regards to the SNR differ? Taking the Friis transmission model [68] into account, the RSS for omnidirectional antennas can be calculated with the distance d , receiving antenna gain G_R , wavelength λ , transmitting antenna gain G_T and transmission power P_T as follows:

$$RSS = P_T * G_T * G_R * \frac{\lambda^2}{(4 * \pi * d)^2}. \quad (5.2)$$

When λ is replaced and P_T , G_T , and G_R are set to 1 the following equation can be derived:

$$RSS = \frac{c^2}{(f * 4 * \pi * d)^2}, \quad (5.3)$$

where c is the speed of light, and f is the transmission frequency. Converting the equation to d results in the following equation:

$$d = \frac{c}{(4 * \pi * f * \sqrt{RSS})}. \quad (5.4)$$

The equation shows that a lower frequency results in a higher RSS for a given distance. This means that the 2.4 GHz band can achieve a higher SNR for a given distance and noise floor compared to the 5 GHz band. The following conclusion can be derived from the equation: The 2.4 GHz band can accomplish a lower PER for a given set of physical layer parameters, distance and noise floor.

The simulation results indicate that modern Wi-Fi offers various physical layer parameters to enhance the robustness of the outdoor communication. The intensity of the impact varies depending on the environment and the actual communication channel. Every physical layer configuration has also an impact on data throughput, which is the next topic to be analyzed.

5.2 Data Rate

For the simulation of Wi-Fi data throughput, various tools are already available, such as Matlab, ns-2 and ns-3, OMNeT++, Qualnet [69] or OPNet [57].

Kumar et al. [57] compares different available simulators for the simulation of wireless networks and concludes that, in general, ns-2, ns-3 and OMNeT++ are the most popular simulators for academic research of wireless networks. Keller, Andre, and Wiedner [69] mentions that ns-3 keeps a more accurate Implementation of the IEEE 802.11 standard than OMNeT++. So far, I know that OMNeT++ supports

some IEEE 802.11ac modes via the library INET Release 4.0.0²¹. Consequently, OMNeT++ seems unsuitable for IEEE 802.11ax simulations and I looked at ns-3.

ns-3 Network Simulator

Ns-3 is well documented in the ns-3 manual in the `./doc` - folder of [70], where I found the following information about the simulator. Ns-3 is a discrete-event network simulator project which was founded in 2006. The ns-3 project is open source with a licence based on GNU GPLv2 compatibility. It aims to provide an open, extensible network simulator for research and educational use. Ns-3 scripts can be written in C++ or Python.

The concept of ns3 is based on the abstraction of simulated systems. For this purpose, the term node was introduced for basic computing devices. The Node class offers the possibility of installing protocol stacks and applications or adding peripheral cards and mobility models to the node. Applications are the abstraction of the user-level applications, representing an activity to be simulated. For this purpose, the applications use resources and functionalities provided by the system software of a node.

Every node gets network access via the Net Device class. The Net Device class represents the physical interface of a node, which can be a network interface card or peripheral card. The Net Device simulates the software driver and the network interface hardware.

Every Net Device is connected to a channel. The channel class represents the physical medium which is used to transmit data. The channel behaviour is based on the channel model, which may include interference, propagation delay and loss.

The current version ns-3.37 supports IEEE 802.11ax as a standard in infrastructure and ad-hoc mode²². However, support for the 802.11ax standard is not yet complete. It is already possible to configure DCM and STBC, but there is a comment in line 496 of the file `he-ppdu.cc` that these are not yet taken into account in the current ns-3 version 3.37²³.

When examining the implementation of 802.11ax in ns-3, one notices that the implementation of 802.11ax in ns-3 already implements a HE ER SU PPDU preamble, but this is never used, and one cannot activate the extended range mode. Therefore, some open points of 802.11ax in ns-3 still need to be implemented.

Black, Gamboa, and Rouil [71] have developed a 3D visualisation of ns-3, which visualises the simulations in 3D to make the ns-3 simulation scenarios tangible. The authors' graphical extension consists of two open source programmes. The

²¹<https://inet.omnetpp.org/2018-06-28-INET-4.0.0-released.html>

²²<https://www.nsnam.org/docs/models/html/wifi-design.html>

²³<https://www.nsnam.org/docs/models/html/wifi-user.html>

NetSimulyzer ns-3 module ²⁴ can be integrated into the ns-3 simulation and builds a JSON file using the specified functions and configurations. This file contains all the data required for visualisation in the application NetSimulyzer ²⁵.

Ns-3 is chosen as a simulation tool for the simulation of 802.11ax by [72], [26] and [31].

As ns-3 is an open-source simulation software and was used by the mentioned other researchers in the past too, I used ns-3 to evaluate the effect of physical layer configuration on the achievable goodput between two nodes using IEEE 802.11ax Wi-Fi Netdevices to exchange UDP packets in ad-hoc Mode.

The setup consists of two nodes placed in static positions with a distance of 20 m. I chose the short communication range setup with no simulated interference to enable Wi-Fi transmission without any packets lost.

Every node is equipped with an IEEE 802.11ax Wi-Fi NetDevice, which is configured with the default parameters in Table 5.2.

General Parameters

Wi-Fi Standard	IEEE 802.11ax
GI	3200 ns
Frequency Spectrum	5.6 GHz
BW	20 MHz
max. Transmission Power	25 dB
Antenna Gain	5 dB
Spatial Streams	2

Table 5.2 – Default simulation parameters for Wi-Fi Devices in the goodput simulations

A Constant Rate Wi-Fi Manager is used to set a constant data rate according to the fixed HE-MCS for data, non-uniform and control data transmissions. The used frequency band is 2.4 GHz or 5 GHz as higher frequencies are less resistant to shadowing and fading, and a higher data rate is not needed for the WIC use cases. The Wi-Fi Netdevices operate in the frequency channels specified in Table 4.1, which can be used for outdoor Wi-Fi communication in Germany [54], [55].

The simulation is based on the ns-3 ConstantSpeedPropagationDelayModel and the ns-3 FriisPropagationLossModel, representing free-space signal propagation at the speed of light. The FriisPropagationLossModel is suitable for outdoor scenarios with a clear LOS between the nodes. As both nodes are only 20 m apart a transmission in the LOS is possible. The ns-3 TableBasedErrorRateModel is used to model the

²⁴<https://github.com/usnistgov/NetSimulyzer-ns3-module>

²⁵<https://github.com/usnistgov/NetSimulyzer>

error rate of the physical layer. According to the ns-3 Wi-Fi design guide²⁶, the TableBasedErrorRateModel derives the PER from results of the Matlab WLAN Toolbox regarding the physical layer parameters and SNR. The design guide recommends the TableBasedErrorRateModel for the IEEE 802.11ax standard.

As the Wi-Fi standard implements ACKs for every packet, every lost packet is repeated until it is received or the number of retries is exceeded. Platooning Services are time critical, so the number of retries should be as low as possible. This is why additional retransmission mechanisms like TCP are not needed. Therefore, the chosen transport layer protocol is UDP.

One node operates a UDP server, and the other is a UDP client. The client sends 1000 Byte UDP packets to the server every 0.1 µs. This packet interval ensures that the packet queue of the client is never empty after starting the simulation. The server receives the packets and sends an ACK back to the client.

For every physical layer configuration, the simulation runs five times for 5 s. The goodput for every simulation run is calculated by dividing the number of received bytes at the UDP Server by the simulation time. The goodput is then averaged over all simulation runs per physical layer configuration, and the confidence interval with a confidence level of 95 % is calculated.

The theoretical data rate for the different physical layer configurations is retrieved from the function ns3::WifiMode::GetDataRate().

To verify the simulation software, I used different methods. First, I confirmed that the theoretical data rate for the simulation's IEEE 802.11ax physical layer configurations equals the theoretical data rate specified in the IEEE 802.11ax standard [16].

I also used the MonitorSnifferRxCallback and the MonitorSnifferTxCallback of the ns-3 WifiPhy class to check the ongoing transmissions. Both Callback functions can be added to WifiPhy objects of Wi-FiNetDevice and are called every time a packet is received or transmitted at the Wi-Fi Netdevice. The function parameters are information about the packet, channel frequency and station ID and an instance of the WifiTxVector class. The WifiTxVector instance in the current ns-3 version 3.37 describes all parameters of the transmission in accordance to the TXVECTOR field of the IEEE 802.11 standard [16]. Additionally, the function parameters of the MonitorSnifferRxCallback contain the signal strength and the noise power of the received packet.

Using the provided information from the MonitorSnifferRxCallback and the MonitorSnifferTxCallback, I was able to comprehend the ongoing transmissions and verify the simulation results.

²⁶<https://www.nsnam.org/docs/models/html/wifi-design.html#default-table-based-error-model-validation>

Guard Interval (GI)

In the first simulation, I varied the GI of the Wi-Fi Netdevices for different HE-MCS values. The results are shown in Figure 5.7. The achieved goodput is plotted against the theoretical data rate for the different GI values. The theoretical data rate is always higher than the achieved goodput of the UDP applications because the channel is also used for ACK and ad-hoc Beacon transmissions. Due to these different transmissions, the goodput is lower than the theoretical data rate.

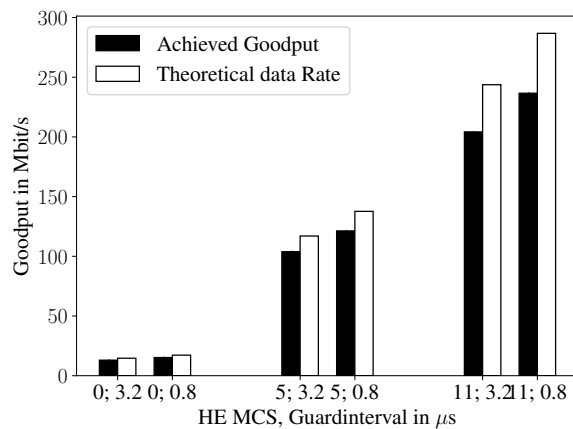


Figure 5.7 – Achieved Goodput and theoretical Datarate of two Wi-Fi6 stations in Ad-Hoc Mode with 2 Multiple Input Multiple Output (MIMO) streams and a bandwidth of 80 MHz in regards to the chosen Guard Interval (GI) and HE-MCS value

The achieved goodput decreases as the GI length increases. This effect can be characterized by Equation 2.1. The bandwidth attenuation for the possible GI lengths is displayed in Table 5.3. The effect of the bandwidth attenuation for the different GI lengths can be observed in the mean achieved goodput in Table 5.3, where the decrease of the mean goodput reflects the bandwidth attenuation of the decreasing GI length.

A similar effect can be observed with higher HE-MCS values.

GI	Mean achieved goodput	BW attenuation
800 ns	31.15 Gbit/s	94 %
1600 ns	29.47 Gbit/s	89 %
3200 ns	26.52 Gbit/s	80 %

Table 5.3 – Bandwidth (BW) attenuation and mean goodput for HE-MCS0 in regards to Guard Interval (GI) length

Patil et al. [63] and Karmakar et al. [73] conducted similar simulations for the 400 ns and 800 ns GI lengths in IEEE 802.11n and IEEE 802.11ac, respectively. Both papers state that shorter GI lengths lead to higher goodput values under the condition that there is a short delay spread and a low channel loss due to interference.

Extended Range (ER) Mode

In the following simulation, I analyzed the effect of the ER Mode on the goodput of the IEEE 802.11ax physical layer. As mentioned in ns-3 Version 3.37, the ER Mode is implemented as a HE Capability with the new extended WifiPreamble. But the new preamble in the HE ER SU PPDU format is not used in ns-3 version 3.37.

As I was using the ConstantRateWifiManager, all parameters for the data transmission are set in the function `ConstantRateWifiManager::DoGetDataTxVector()`. The function creates a `WifiTxVector` instance with the parameters of the transmission. There I overwrote the preamble type to the already implemented ns3 `WifiPreamble::WIFI_PREAMBLE_HE_ER_SU`, when the ER Mode is enabled and conditions for the ER Mode in the IEEE 802.11ax standard [16] are fulfilled. Ns-3 version 3.37 implements the `ns3::GlobalValue`, which allows users to set global values for the simulation, which can be accessed in every class without changing Constructor or function parameters. This leaves the original functionality of the ns3 code intact.

I used the `ns3::GlobalValue` to create an instance named `HE_ER_Mode`, which is set to true at the start and read in the `ns3::ConstantRateWifiManager::DoGetDataTxVector()` function to overwrite the preamble type.

Via the `MonitorSnifferRxCallback` and the `MonitorSnifferTxCallback`, I was able to verify that the `ns3 WifiPreamble::WIFI_PREAMBLE_HE_ER_SU` was used for data transmission, when the following conditions were met: a) the ER Mode is enabled, b) the number of spatial streams is 1, c) the HE-MCS value is less than 3 and d) the BW is 20 MHz.

The simulation results are shown in Figure 5.8, where the reduction of achieved goodput is plotted against the theoretical data rate for the different HE-MCS values. The lost goodput is calculated by subtracting the achieved goodput when using the HE ER mode from the achieved goodput when using the normal HE SU mode. The only difference between HE SU and HE ER SU transmissions is the preamble, which repeats the HE-SIG-A field in the HE ER SU PPDU format. This results in a longer transmission time, reflecting the lower achieved goodput for the ER Mode.

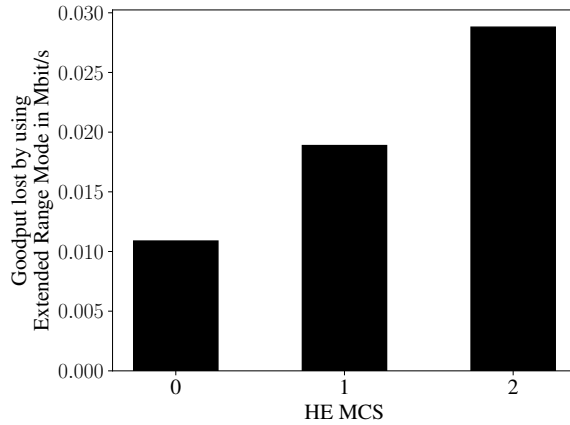


Figure 5.8 – Achieved Goodput and theoretical Datarate of two Wi-Fi6 stations in Ad-Hoc Mode with a Guard Interval (GI) of 3200 ns and a bandwidth of 20 MHz in regards to the number of Multiple Input Multiple Output (MIMO) streams and the chosen HE-MCS value

The effect increases with smaller packet sizes because the longer preamble transmission time is more significant for smaller packets. For higher HE-MCS values, more achievable goodput is lost because longer transmission time for the preamble could have been used more OFDM symbol transmissions, where more data is coded onto a symbol.

Dual Carrier Modulation (DCM)

Using the DCM in the IEEE 802.11ax physical layer also affects the achievable goodput. As aforementioned, the DCM is not supported by ns-3 version 3.37. Therefore, I implemented the DCM for this simulation in the ns-3 version 3.37 by transmitting a payload of twice the size, which represents the original payload and a copy of it for the HE-MCS values 0, 1, 3 and 4, where MCS is allowed. Using DCM, the receiver would apply maximum likelihood decoding to decode the original payload with a higher probability.

The results of the simulation are shown in Figure 5.9, where the lost achieved goodput is plotted against the theoretical data rate for the different HE-MCS values. The theoretical data rate while using DCM is half of the theoretical data rate without DCM, which complies with the IEEE 802.11ax standard [16].

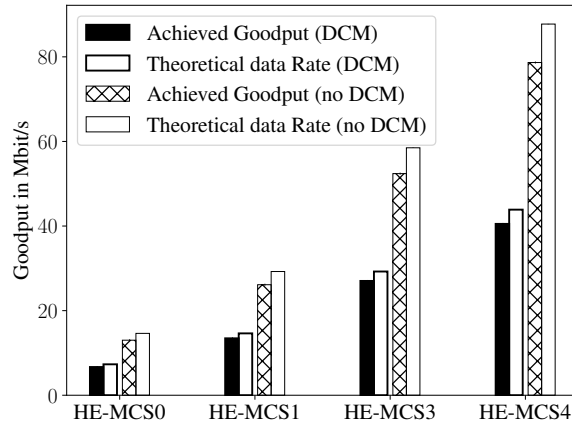


Figure 5.9 – Achieved Goodput and theoretical Datarate of two Wi-Fi6 stations in Ad-Hoc Mode with for IEEE 802.11ax physical layer parameters of a Guard Interval (GI) of 3200 ns, a Bandwidth (BW) of 20 MHz and 2 spatial streams in regards to the number of the chosen HE-Modulation and Coding Scheme (MCS) value and whether Dual Carrier Modulation (DCM) is enabled

The achieved goodput is always lower than the theoretical data rate because data transmission time is lost to the header overhead and media access time. Wi-Fi access is based on CSMA/CA, meaning the stations have to wait for a random time before transmitting on a free channel. Additionally, the channel can be occupied by ACK or ad-hoc beacon frames, which must be transmitted.

Using DCM increases the ratio of achievable goodput to theoretical data rate because only one header and one ACK frame are transmitted per 2000 Byte payload, and the node has to go to the medium access procedure only once per 2000 Byte payload.

Space-Time-Block-Code (STBC)

Another physical layer parameter that reduces the theoretical data rate for more robustness is the STBC. As mentioned, ns-3 version 3.37 does not support the STBC for the IEEE 802.11ax standard. Therefore, I reduced the number of MIMO streams from 2 to 1 when the STBC is enabled. STBC would transmit a redundant copy of the data on the second antenna, which would be combined using the space-time block code (STBC) to increase the robustness and reliability of the transmission. The results of the simulation are shown in Figure 5.10, where the lost achieved goodput is plotted against the theoretical data rate for the different HE-MCS values. The theoretical data rate while using STBC is half of the theoretical data rate without STBC, which complies with the IEEE 802.11ax standard [16].

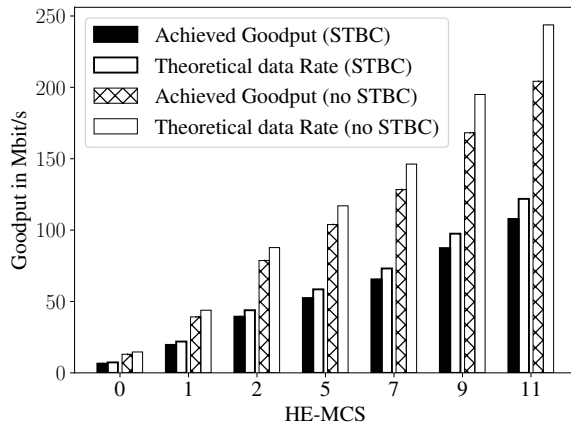


Figure 5.10 – Achieved Goodput and theoretical Datarate of two IEEE 802.11ax stations in Ad-Hoc Mode with for IEEE 802.11ax physical layer parameters of a Guard Interval (GI) of 3200 ns, a Bandwidth (BW) of 20 MHz and 2 spatial streams in regards to the number of the chosen HE-Modulation and Coding Scheme (MCS) value and whether Space-Time-Block-Code (STBC) is enabled

Other physical layer parameters, supported by the IEEE 802.11ax standard, are LDPC and utilizing more MIMO streams. The effect that using more MIMO streams for transmission increases the achievable goodput, is already known [14]–[16, pp. 294–296]. LDPC adds no new effect for the achievable goodput, but more robustness which results in a lower PER.

Using a different frequency spectrum, the achievable goodput can be limited due to the lower maximum BW of 40 MHz in the 2.4 GHz frequency spectrum. To analyze achievable goodput in the 2.4 GHz frequency spectrum, I reran the simulations with the same configuration as in Figure 5.2, but within the 2.4 GHz frequency spectrum. The results indicate that the achievable goodput is between 0.1 Mbit/s... 2.7 Mbit/s slower than in the 5 GHz frequency spectrum.

Due to a signal extension of 6 μ s in the 2.4 GHz frequency spectrum, the transmission time is longer, which results in a lower achievable goodput. [39] states that the signal extension in the 2.4 GHz frequency spectrum enables backwards compatibility with the older 802.11 standards, which need time to write their network allocation vector register.

The simulation results represent an ideal scenario where only two nodes exchange data. In a real-world scenario in the agricultural domain, the number of nodes and the distance between the nodes may be higher. The signal propagation will be influenced by the complex agricultural environment, which can consist of large water areas, various obstacles and vegetation or weather conditions [47]. In case of the corn harvest scenario, Smolnik and Lücke [11] points out that corn plants

can be up to 3 m high and thus influence signal propagation. These factors in the real-world scenario can lead to higher PER and thus reduce the achievable goodput.

5.3 Link Level Simulation Evaluation

The past two sections gave an overview of impact of the different parameters on the achievable goodput and robustness of the IEEE 802.11ax standard. Both simulations were based on nearly ideal conditions, where the channel was not affected by any interference from other devices.

The results show the complex interplay of the different parameters in regards of the achievable goodput and robustness. Every mentioned parameter can be set to have the highest possible data rate, which may lead to a low robustness and vice versa. When the communication link is less robust, more retransmissions are required, which may result in a lower goodput. When the configured data rate is too low, the goodput is also reduced.

As every application has different requirements on latency, range, robustness and goodput, the parameters can be configured accordingly.

In general, modern Wi-Fi offer a variety of different parameters, to achieve the best possible performance for the specific application. The new IEEE 802.11ax ER mode combined with DCM offers the highest robustness at low SNRs according to my simulations, which can be used for long range applications. The robustness simulation indicated, that the ER mode and DCM could extend the range, which was measured in the field experiment.

To deal with intersymbol interferences due to multipath effects, which were considered as the main reason for a high PER in Wi-Fi outdoor networks by [49] and [50], IEEE 802.11ax offers longer GIs of up to 3200 ns. My simulations show that GI of 3200 ns is more robust against multipath effects than GI of 800 ns, but reduces the theoretical achievable data rate.

Since IEEE 802.11n, the robustness of the communication link can be increased by applying STBC. But just as the IEEE 802.11ax DCM mode, the increased robustness comes at the cost of a reduced theoretical data rate.

The following chapter analyses the impact of the different physical layer parameters on the latency of the Application Layer.

Chapter 6

Application Level Simulation

6.1 Agricultural Platooning Services

After I analyzed the impact on data rate and robustness of the physical layer parameters, I will simulate a platooning scenario in ns-3 to find the influence of the physical layer configuration on the network performance.

The network performance metric consists of the latency, which describes the time needed to transmit the data on the application layer, and the update rate of the platooning service, which defines how long ago a new position update was received by the TM in the Platooning Service.

Ns-3 is suitable for this simulation because it supports application layer-level simulation. Via the extension Netsimulyzer, a graphical user interface is available to visualize the simulation results.

Any packets in ns-3 can be tagged with a ns-3 Packet Tag²⁷, which are designed to add additional information to the packet. Every added ns-3 Packet Tag belongs to the packet and does not change the packet size or characteristics. Throughout the simulation, I used ns-3 Packet Tags to add information that needed transferring.

The simulation scenario is based on the corn harvest and loading scenario, which is described in section 2.2, where multiple FHs harvest the corn and load it onto one of the TMs.

An ns-3 Node represents every machine. Each Node has a mobility model, which describes the movement of the machine.

Wi-Fi Setup

In order to exchange data between the machines, every machine is equipped with an ns-3 IEEE 802.11ax WifiNetDevice. Every Wi-Fi Device runs in Ad-Hoc mode to

²⁷https://www.nsnam.org/docs/release/3.36/doxygen/classns3_1_1_tag.html

enable direct communication between the machines. The Wi-Fi data rate is managed by a Constant Rate Wi-Fi Manager, which has a non-uniform transmission mode and a data mode for uniform transmissions. The transmission modes are configured according to the parameters in Table 6.1.

The parameters are chosen from the results of the physical layer analysis of section 5.2 and section 5.1. Non-uniform transmissions are used to broadcast the Agricultural Platooning Service advertisements.

The non-uniform transmission parameters enable the longest possible transmission range, which results in the lowest data rate. Since no high data rate is required to advertise the Service, I chose the parameters to maximize the transmission range. As aforementioned, ns-3 does not support DCM at the moment. In order to implement DCM in the simulation, I doubled the data length for DCM enabled transmissions to represent the overhead of transmitting redundant copies of data for DCM. DCM would utilize the copies to determine the correct data via maximum likelihood decoding. As a result, the communication would be more robust, as shown in section 5.1. This effect is not included in the current version of the simulation.

Guidance data in the Agricultural Platooning Service is exchanged between the FH and the TM via the uniform transmission mode. The process data in chapter 3 reflects that a short transmission range is sufficient to exchange the guidance data, which must still be robust against multipath effects. I chose the parameters to balance a high robustness and high data rate. The uniform transmission parameters are changed in the simulation to analyze the impact on the network performance metrics.

Similar to the ns-3 simulation in section 5.2, this simulation is based on the ns-3 ConstantSpeedPropagationDelayModel, the ns-3 FriisPropagationLossModel and the ns-3 TableBasedErrorRateModel.

General Parameters

Wi-Fi Standard	IEEE 802.11ax
GI	3200 ns
LDPC enabled	True
Frequency Spectrum	5.6 GHz
BW	20 MHz
Max. Transmission Power	25 dB
Antenna Gain	5 dB
Maximum retries	3

Uniform Transmission Parameters

MCS	5
Number MIMO Streams	2

Non-Uniform Transmission Parameters

Broadcast MCS	0
ER mode enabled	True
DCM enabled	True

Table 6.1 – Default simulation parameters for Wi-Fi Devices on Forage Harvester (FH) and Transport Machine (TM)

Agricultural Platooning Service

Every machine node runs an ns-3 Application responsible for the Agricultural Platooning Service. The application is identified by a unique identifier and runs a UDP socket to exchange data with other Agricultural Platooning Service applications. Every UDP socket can be addressed by an IP address and a port number. The IP address is the IP address of the machine node.

Every FH starts in the lower left corner of the field and harvests the corn along the path, which is displayed in Figure 6.1. As soon as a FH reaches a field border, it makes a U-turn and continues in the opposite direction. Every FH harvests the corn until it reaches the end of the field in the lower right corner. The initial position of the TMs is a row below the FHs, which is displayed in Figure 6.2.

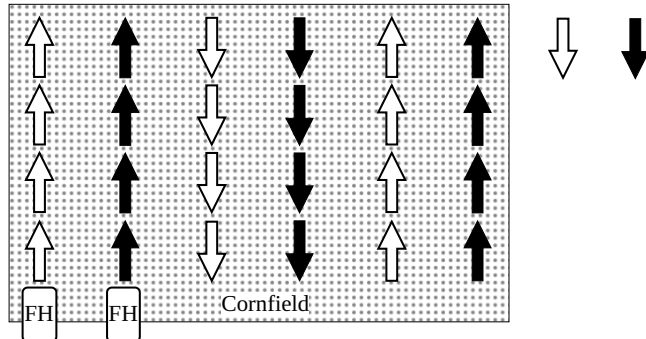


Figure 6.1 – Path of the Forage Harvester (FH) for harvesting corn on the field

In the beginning, every FH broadcasts a search request *search_TM* via the non-uniform transmission mode to find an empty TM to load the corn onto according to the procedure in Algorithm 6.1. As shown in Figure 6.2, multiple TMs receive the search request and answer with their current fill level of the TM's trailer. The FH chooses the TM with the lowest fill level and sends a connection request to the TM. As soon as the TM receives the connection request, it answers with a connection response. When the FH receives the connection response, the Agricultural Platooning Service is started. When no TM answers the search request, the FH repeats the search request every *search_TM_interval* seconds.

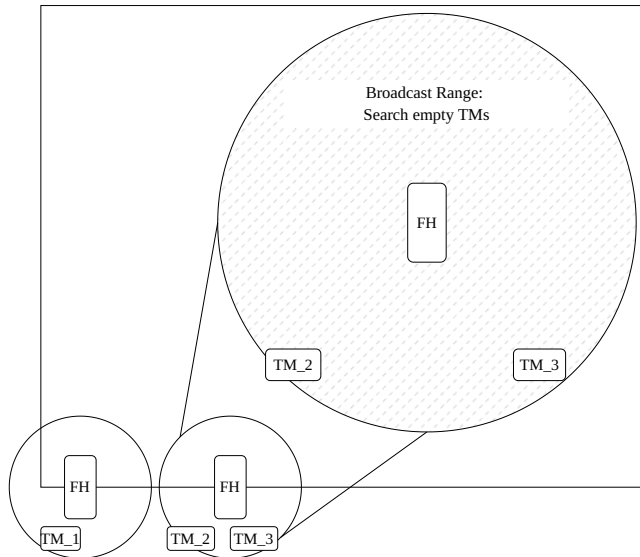


Figure 6.2 – Start position of the Forage Harvester (FH)s and Transport Machine (TM)s, where a FH broadcasts a search request to find a TM to load the corn onto

Next, the FH starts to harvest the corn. All steps of the harvest process and Agricultural Platooning Service are summarized in Algorithm 6.2.

The FH harvest process is defined by the harvest states in Table 6.2, where every harvest state represents a different PD and FH speed, which are derived from the key figures of a FH harvesting corn with a working width of 6.2 m on a 80 ha field in [7]. When the PD is low, the FH can harvest faster and vice versa.

Starting in the harvest state H1, the FH determines the next harvest state every 50 ms by the Markov chain in Figure 6.3. This Markov chain ensures that the harvest

Require: Defined *search_TM_interval*, *search_TM_packet_length*

- 1: Create packet *search_TM* of length *search_TM_packet_length* bytes
- 2: Broadcast *search_TM* to all TMs
- 3: **if** no TM answers **then**
- 4: Repeat Broadcasting *search_TM* every *search_TM_interval* seconds
- 5: **else**
- 6: Send connection request
- 7: **if** No TM response **then**
- 8: Repeat Broadcasting *search_TM* every *search_TM_interval* seconds
- 9: **else**
- 10: Connection established
- 11: Start Agricultural Platooning Service
- 12: **end if**
- 13: **end if=0**

Algorithm 6.1 – Procedure of the Forage Harvester (FH) to search for a Transport Machine (TM) to load the corn onto

Require: Defined *platoon_data_interval*, *platoon_data_packet_length*

- 1: Calculate harvested volume
- 2: Advance FH position
- 3: Add harvested volume to TM fill level
- 4: **if** TM fill level is full **then**
- 5: Disconnect from current TM
- 6: Start Agricultural Platooning Service with waiting TM
- 7: **else**
- 8: Create packet *TM_data* of length *platoon_data_packet_length* bytes, which contains the TM fill level and the new guidance position
- 9: Send *TM_data* to TM
- 10: **if** TM fill level is half full **then**
- 11: Start Algorithm 6.1 to search for new TM
- 12: **end if**
- 13: **end if=0**

Algorithm 6.2 – Procedure of the Forage Harvester (FH) to send the Transport Machine (TM) fill level and the TM guidance position every *platoon_data_interval*

state can't transverse from H0 to H2 directly, which would represent a low PD immediately followed by a high PD. As I do not have enough harvest process data, which contain the PD and the FH speed, I chose the transition probabilities to the best of my knowledge. In future work, process data can be used to determine the transition probabilities.

Harvest State	PD	FH speed
H0	20 t/ha	8.06 km/h (2.24 m/s)
H1	30 t/ha	8.06 km/h (2.24 m/s)
H2	50 t/ha	6.65 km/h (1.845 m/s)

Table 6.2 – Corn harvest states, which define a range of Plant Density (PD)s and Forage Harvester (FH) speeds, where the data is based on the key figures [7]

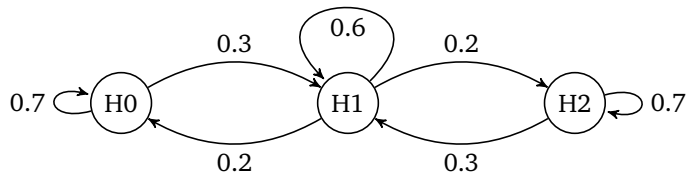


Figure 6.3 – Markov Chain for the Harvest States 0, 1 and 2, which represent the current PD and harvest speed from Table 6.2

After determining the next harvest state, the FH sets the PD and the FH speed according to the defined values in Table 6.2. The position of the FH is advanced by the FH speed multiplied with 50 ms along the harvest path in Figure 6.1. The harvested volume during this *platoon_data_interval* is calculated with the following equations:

$$\text{Harvested Area} = \text{Harvest width} \times \text{Harvest speed} \times \text{Time step}, \quad (6.1)$$

$$\text{Harvested Volume} = \text{Harvested Area} \times \text{PD} \times \text{Corn volume per tonne}. \quad (6.2)$$

The harvested area is represented in ha, and the harvested volume is defined in m³. The needed parameters for the calculation are from [7] and are listed in Table 6.3. The calculated harvested volume is added to the TM's fill level, which is tracked by the FH's application. Keeping track of the fill level represents the knowledge of the FH about the TM's fill level, which the FH would normally get through a sprout guidance system.

Next, the FH determines whether the TM is full. If the TM is full, the FH stops harvesting and sends a disconnect request to the TM. The TM answers with a disconnect response and leaves the field to unload the corn, as shown in Figure 6.5.

If the TM is not full, the FH sends the *TM_data* to the TM, which contains the new TM fill level and the new guidance position. The TM updates the fill level and drives to the new position to load the corn, as shown in Figure 6.4. The guidance data positions the TM always 5 m left of the FH because this part of the field was already harvested. The distance between the FH and the TM is as the FH and the TM moved mostly with a distance of around 5 m in the recorded process data in chapter 3.

If the TM fill level is half full, the FH starts Algorithm 6.1 to search for a new TM to load the corn onto. This process is visualized in Figure 6.4. As soon as the FH finds a new TM, the FH connects to the new TM and starts sending the TM guidance positions, which place the TM 12 m behind the FH. The FH continues harvesting until the TM is fully loaded. Meanwhile, the new TM is waiting behind the FH and can take over the loading position next to the FH as soon as the TM, where the FH is currently loading onto, is full.

A fully loaded TM leaves the field to unload the corn and returns to the position where it disconnected from the FH. There, it waits for an incoming *search_TM* request from a FH to connect to a FH again.

The corn harvest process is finished when the last FH has finished harvesting and moved to the end of the field as shown in Figure 6.1.

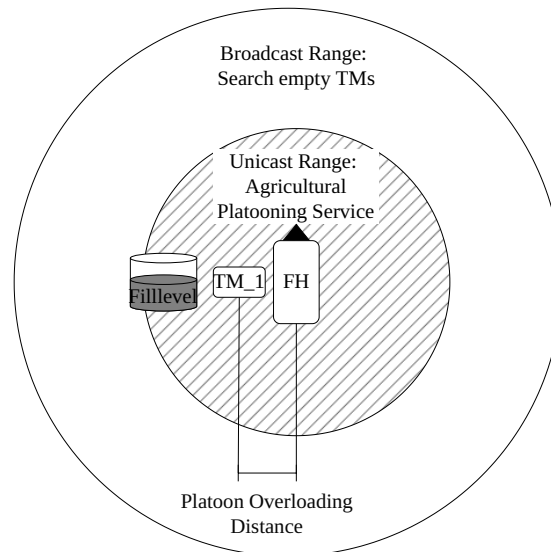


Figure 6.4 – Transport Machine (TM) position left of the Forage Harvester (FH) for overloading, where the TM is half full and the FH starts Algorithm 6.1 to search for a next empty TM, which can later take over the loading position.

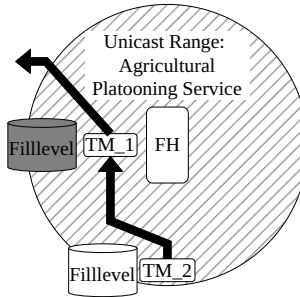


Figure 6.5 – Change of Transport Machine (TM)s in the Application Agricultural Platooning Service, where TM_1 is full and leaves the field while the empty TM_2 takes over the overloading position.

Parameters	
<i>search_TM_interval</i>	1 s
<i>search_TM_packet_length</i>	0.5 kByte
<i>platoon_data_interval</i>	50 ms
<i>platoon_data_packet_length</i>	1 kByte
Platoon Overloading Distance	5 m
FH Working Width	6.2 m
TM Volume	50 m ³

Table 6.3 – Simulation parameters for the Application Agricultural Platooning Service

Simulation Verification

Each corn harvest scenario is visualized to ensure the correctness of the simulation. The visualizations are created with the ns-3 extension Netsimulyzer. The corn field is marked as a black rectangle. Next to the lower left corner there is a cuboid which marks the location of the silo. Every node was displayed as the Netsimulyzer model of a landdrone, where all FHs are black and the TMs are either red, green, yellow or blue, depending on the TM state.

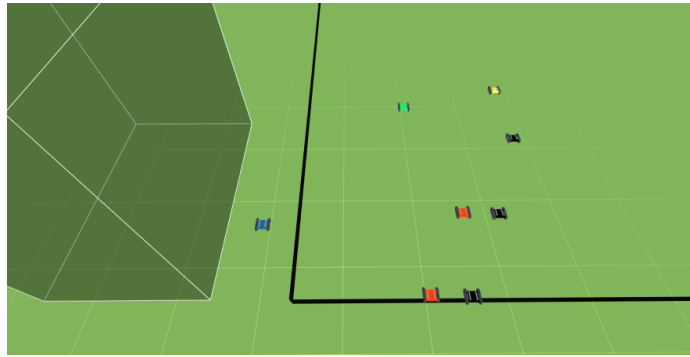


Figure 6.6 – Screenshot of the simulation visualization in Netsimulyzer, where a blue Transport Machine (TM) is unloading in the back in front of the farm cuboid, two red TMs are in a Agricultural Platooning Service with the black Forage Harvester (FH)s, a green TM is empty and waiting for a new *search_TM* request and a yellow TM is in waiting position behind a black FH.

An empty TM is displayed green and changes to yellow as soon as it is associated with a FH and in waiting position behind the FH. The TM is red as soon as the FH starts loading the corn onto the TM in an Agricultural Platooning Service. A full TM is displayed blue and moves to the farm cuboid next to the lower left corner of the field. As soon as the TM is empty, it changes back to green and waits for a new FH to connect to it at the last disconnection position.

I use this visualization to verify the correct mobility of the FH and the TM, the correct TM state transitions, that the simulation is ending properly and that the FH switches the waiting TM after disconnecting from the fully loaded TM.

Using the provided information from the ns-3 MonitorSnifferRxCallback and MonitorSnifferTxCallback I was able to review ongoing transmissions and whether the specified physical layer parameters are used correctly for non-uniform and uniform traffic.

Every simulation runs 2 TMs per FH. This does not correspond to the key figures of 10 TMs per FH in the corn harvest scenario [7], but is sufficient as there is no communication of TMs while transporting the harvested crop to the farm currently planned. For this reason, I have set the simulation so that a full TM is empty again after 10 s at the disconnect position. This is a reasonable value, as it ensures that every time a FH starts a *search_TM* request, there is a TM in range to connect to.

Zhang et al. [8] defined a data frame of 32 Byte, which includes an identifier, timestamp, longitude, latitude, heading, speed and direction. This set of data comprises a basic set which is sufficient for the implementation of a platooning service, as the authors show. Schlingmann and Benishek [2] do not specify the amount of data further and point out that the required data rate for platooning services is low.

The use case requirements for vehicle platooning services in [74] specify data sizes of 300 kByte ... 1200 kByte, depending on the vehicle density.

I have set the data size *platoon_data_packet_length* to 1 kByte for the simulation of platooning services. This data size is an abstraction of the storage space that may be needed for additional data or implementations of authentication and security mechanisms. In the Corn Harvest scenario, additional data could be, for example, the fill level of the transport machine, information about the environment, obstacles or other machines on the field.

Zhang et al. [8] already showed that an interval of 100 ms is sufficient for Agricultural Platooning Services in a harvest scenario.

I chose a *platoon_data_interval* of 50 ms for the Agricultural Platooning Service as Smolnik and Lücke [11] mention that their requirements analysis indicated that new guidance data should at least arrive every 50 ms.

6.2 Application Level Simulation Evaluation

I chose the following simulation configurations for the uniform transmission of guidance data: HE-MCS 3, 5 and 7 and STBC either enabled or disabled. Every simulation configuration runs 5 times, where every FH harvests 1 ha of corn, which equals to roughly 2.5 TM loads. Every simulation run has a different random seed. After the simulation run successfully and the simulation process is verified in the visualization, a mean value and confidence interval with a confidence level of 95 % is calculated per simulation configuration.

The results for defined metrics latency and data update rate are shown in Figure 6.7.

The desired *platoon_data_interval* of 50 ms can be achieved with every configuration.

The confidence interval for the mean update rate is always below 2 μ s. The mean latency is always below 0.4 ms. Using higher HE-MCS values reduces the mean latency of the Agricultural Platooning Service data exchange.

Applying STBC additionally increases the mean latency compared to non-STBC configurations. This is due to the fact that the STBC configuration uses the redundant copy of data to improve the reliability of the transmission by applying maximum likelihood decoding. This decreases the data rate and increases the mean latency. Nevertheless, the desired *platoon_data_interval* of 50 ms can be achieved when using STBC for every specified HE-MCS value and thereby increase the reliability of the transmission.

The recorded process data from the corn harvest scenario showed that the FH can also harvest at higher speeds around 10 km/h than the key figures in [7] report.

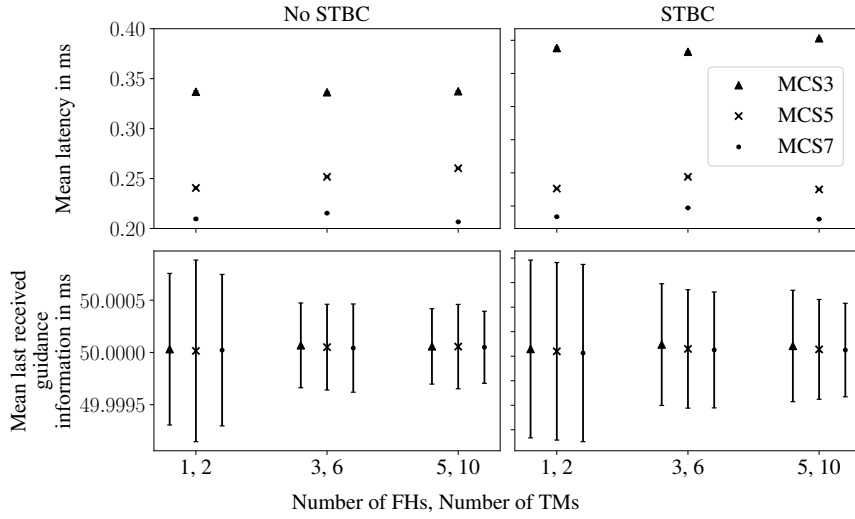


Figure 6.7 – Mean latency and mean guidance data update interval of the Application Agricultural Platooning Service in regards to the number of FHs and TMs and the chosen HE-MCS value for a *platoon_data_interval* of 50 ms.

To test the applicability of the Agricultural Platooning Service for higher speeds, I ran a additional simulation where I changed the harvest states according to Table 6.4.

Harvest State	PD	FH speed
H0	20 t/ha	14 km/h (3.89 m/s)
H1	30 t/ha	12 km/h (3.33 m/s)
H2	50 t/ha	10 km/h (2.78 m/s)

Table 6.4 – Corn harvest states, which define a range of Plant Density (PD) from [7] and Forage Harvester (FH) speeds, which I set higher than the key figures in [7] specify to increase the requirements on the Agricultural Platooning Service.

As I increased the FH speed, which leads each harvest platoon, the whole platoon harvests the field faster. Therefore, all TMs move faster. To provide faster TMs more often with guidance data, I decreased the *platoon_data_interval* to 25 ms to ensure, that a TM always stays in the harvest platoon position even at higher speeds.

This *platoon_data_interval* of 25 ms heads in the direction of the upper required update rate of 10 ms...25 ms for general vehicle platooning services in [74]. But the values in [74] correspond to higher platoon sizes, a velocity of 100 km/h and a vehicle distance of 1 m...2 m.

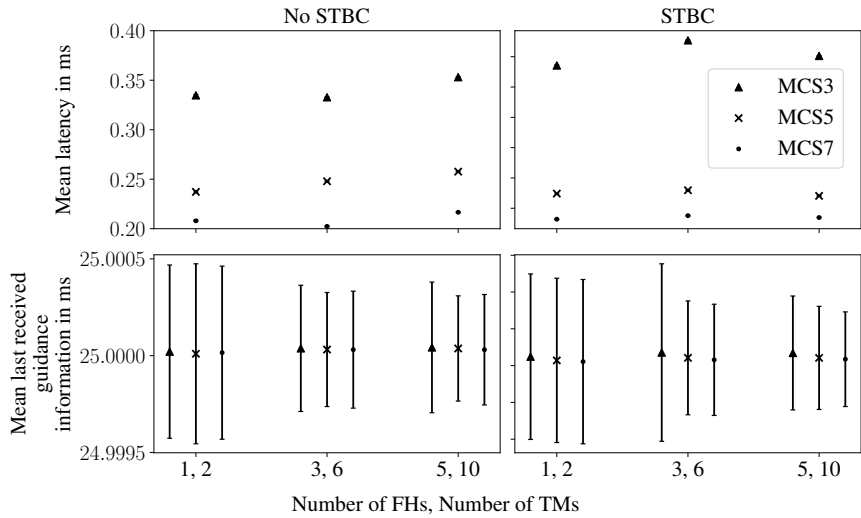


Figure 6.8 – Mean latency and mean guidance data update interval of the Application Agricultural Platooning Service in regards to the number of FHs and TMs and the chosen HE-MCS value for a *platoon_data_interval* of 25 ms.

The simulation runs with the same physical layer configurations as in Figure 6.7. The results displayed in Figure 6.8 reveal that the mean guidance data update interval is always around 25 ms, which is the desired *platoon_data_interval*. The mean latency is nearly the same as in Figure 6.7, which indicates that there is still some channel capacity left for further data exchange.

Both simulations were based on the abstracted and simplified corn harvest scenario, which is based on the ns-3 communication model and abstracted implementation of the physical layer and MAC layer in ns-3. In a real-world scenario, an Agricultural Platooning Service has to operate in the complex agricultural environment, which may impact signal propagation and communication performance.

The simulated communication is based on a BW of 20 MHz, which offers the highest possible signal power spectral density. Additional robustness is gained by using STBC, LDPC, low MCS values and CRs which are encoded for example in HE-MCS3 and are available since the IEEE 802.11n standard. These physical layer configurations are enough to transmit guidance data in an Agricultural Platooning Service.

Both simulations did not consider the impact of interference due to other ongoing transmissions. For example, WIC Video streaming services can increase the network load and consequently lead in higher latencies for the Agricultural Platooning Service. A solution would be to prioritize the Agricultural Platooning Service over other services to ensure a certain quality of service. When passing houses, industrial, or farm buildings, additional Wi-Fi transmissions can be expected. Interference with

other Wi-Fi transmissions can easily occur, when the channel is heavily loaded. The results showed that some channel capacity is still left for further data exchange of other channel users. Since a narrow bandwidth of 20 MHz is used, interference is less likely compared to wider bandwidths, as a wider spectrum is likely to be more utilised if transmission in the frequency spectrum are equally distributed.

Using IEEE 802.11ax, a new service discovery transmission mode is available. Additionally, to the lowest MCS and CR, IEEE 802.11ax can apply the ER mode with DCM which increases robustness as shown in section 5.1 and therefore increases the communication range. This physical layer amendment is designed to introduce a new level of long-range communication in IEEE 802.11. At the moment, I am not aware of any research that measured the resulting communication range in an agricultural environment.

If the communication range is not sufficient for service discovery, a road side unit at the field entrance can be used to exchange FH position data between TMs leaving and entering the field. Alternatively, a field planner can be used to give an overview of where a FH should be harvesting, when everything works as expected. These two options can provide FH position estimations, which can be used to guide TMs to a position where they are likely to receive service discovery broadcasts from FHs.

Chapter 7

Conclusion

This thesis investigates the suitability of modern Wi-Fi for Wireless-Infield Communication (WIC), which describes a wireless process data exchange between agricultural machines in the field. The investigation is based on the prototypical application Agricultural Platooning Service in the corn harvest scenario, which exchanges guidance data via WIC to lead Transport Machine (TM)s to the overloading positions of forage from Forage Harvester (FH)s.

I analyzed corn harvest process data, which indicated that the overloading position is usually at a distance below 10 m at every angle relative to the FH.

A field measurement campaign in a farming environment indicated Wi-Fi communication can range up to 2500 m in a line-of-sight scenario. However, signal strength can suffer from multipath, shadowing and fading effects due to the agricultural environment and the machine sizes. Therefore, Wi-Fi rate managers should be configured to enable robust communication instead of maximizing the data rate.

I simulated different Wi-Fi physical layer configurations to analyze their impact on data rate and robustness. IEEE 802.11ax introduces the new Extended Range (ER) mode, enabling robust and long-range communication for service discovery transmission when used with Dual Carrier Modulation (DCM). The Guard Interval (GI) of 3.2 μ s in IEEE 802.11ax can be used to combat intersymbol interferences due to multipath effects in the agricultural environment. The guidance data exchange mode can be configured to use low Modulation and Coding Scheme (MCS) like High-Efficiency (HE)-MCS3 with Space-Time-Block-Code (STBC) and low-density parity-check (LDPC) to achieve a robust communication, which enables the WIC to meet the required latencies and message intervals for Agricultural Platooning Services in the corn harvest scenario.

In this thesis, I showed that IEEE 802.11ax provides many configurations to enable robust communications which meet the requirements of the use case Agricultural Platooning Services.

List of Abbreviations

ACK	Acknowledgement
AEF	Agricultural Industry Electronics Foundation
AP	Access Point
BCC	binary convolutional coding
BSS	Basic Service Set
BW	Bandwidth
CH	Combine Harvester
CR	Coding Rate
CSMA/CA	Carrier Sense Multiple Access/Collision Avoidance
CTS	Clear-to-Send
DCF	Distributed Coordination Function
DCM	Dual Carrier Modulation
DIFS	Distributed Coordination Function Interframe Space
EDCA	Enhanced Distributed Channel Access
ER	Extended Range
ESS	Extended Service Set
FEC	Forward Error Correction
FH	Forage Harvester
FMIS	Farm Management Information System
GI	Guard Interval
GPS	Global Positioning System
HE	High-Efficiency
HT	High-Throughput
IBSS	Independent Basic Service Set
IFS	Interframe Space
LDPC	low-density parity-check
LOS	Line-Of-Sight
M2M	Machine-To-Machine
MCS	Modulation and Coding Scheme
MIMO	Multiple Input Multiple Output

MU	Multi-User
NAV	Network Allocation Vector
OFDM	Orthogonal Frequency-Division Multiplexing
OFDMA	Orthogonal Frequency-Division Multiple Access
PCF	Point Coordination Function
PD	Plant Density
PER	packet error rate
PPDU	Physical layer convergence protocol data unit
PSK	Phase Shift Keying
QAM	Quadrature Amplitude Modulation
RSS	Received Signal Strength
RTS	Request-to-Send
RU	Resource Unit
SIFS	Short Interframe Space
SNR	Signal Noise Ratio
SSID	Service Set Identifier
STA	station
STBC	Space-Time-Block-Code
SU	Single-User
TM	Transport Machine
UDP	User Datagram Protocol
V2X	Vehicle-to-everything
VHT	Very-High-Throughput
WIC	Wireless-Infield Communication
WPA	Wi-Fi Protected Access

List of Figures

2.1 Forage Harvester (FH) and Transport Machine (TM) in a corn harvesting and loading process	5
2.2 Lateral and longitudinal offset between the two agricultural machines Forage Harvester (FH) and Transport Machine (TM) in a corn harvest scenario	6
2.3 Decrease in the agricultural labor force in Germany based on the data from [10]	7
2.4 Receiver minimum input level sensitivity for different HE-MCS values according to [16], where packet error rate (PER) is less than 10 % . .	15
2.5 Hidden Station Problem, where interferences at the Access Point (AP) can occur, when station (STA) A and B send simultaneously	18
2.6 Data transmission between a sender and receiver in regards to the time with normal Acknowledgement (ACK) 2.6a, fragmentation 2.6b and additional Block Acknowledgement (ACK) 2.6c	19
3.1 A FH and a TM in harvest and overloading scenario, which is represented as distance and speed data plotted in regards to the time and which is visualised as a black and white travel lane for the FH, TM respectively	27
3.2 Distribution of time proportions where a given distance was between Forage Harvester (FH) and Transport Machine (TM) in a harvest platoon scenario.	28
3.3 Distribution of time proportions where Forage Harvester (FH) and Transport Machine (TM) drove with a certain speed in a harvest platoon scenario	28
3.4 Relative bearing between FH and TM which is calculated using the previous location of FH by using β and α for Equation 3.1	29
3.5 Distribution of time proportion at specific distances and relative bearings between Forage Harvester (FH) and Transport Machine (TM) . .	30

3.6 Forage Harvester (FH) and Transport Machine (TM) start cutting a new field section	30
4.1 Path around the static Combine Harvester (CH), which the Transport Machine (TM) will drive during the experiment to mimic various overloading positions	33
4.2 Wi-Fi transmissions between the Wi-Fi Access Point (AP) on the Transport Machine (TM) and the Wi-Fi station (STA) on the Combine Harvester (CH), which are recorded by a third Wi-Fi device in monitor mode on the Combine Harvester (CH)	34
4.3 Position of the Wi-Fi Devices on the TM and the Combine Harvester (CH) during the trialrun	35
4.4 All QoS data transmissions between the Wi-Fi Access Point (AP) on the Transport Machine (TM) and the Wi-Fi station (STA) on the Combine Harvester (CH) in a trial run, which were initiated by the iperf3 client on the Transport Machine (TM)	36
4.5 Airfield near Mahlwinkel ($52^{\circ}23'17.9''\text{N}$ $11^{\circ}50'35.4''\text{E}$) in Saxony-Anhalt, Germany, where I conducted the range measurements	37
4.6 Setup of the Wi-Fi devices for the range measurements, which I mounted on wooden antenna masts to reach a height of 4 m, the maximum allowed height of agricultural machines in Germany	38
4.7 Range measurement results of the Wi-Fi transmissions on the airfield near Mahlwinkel ($52^{\circ}23'17.9''\text{N}$ $11^{\circ}50'35.4''\text{E}$) in Saxony-Anhalt, Germany	38
5.1 Simulated PER regarding SNR for chosen HE-MCS values for IEEE 802.11ax physical layer parameters of a GI of 3200 ns, a bandwidth of 20 MHz and 2 spatial streams.	45
5.2 Simulated packet error rate (PER) in regards to Signal Noise Ratio (SNR) for chosen HE-MCS values and whether LDPC or binary convolutional coding (BCC) is enabled for IEEE 802.11ax physical layer parameters of a GI of 3200 ns, a bandwidth of 20 MHz and 2 spatial streams	46
5.3 Simulated packet error rate (PER) in regards to Signal Noise Ratio (SNR) for chosen HE-MCS values and whether a GI of 800 ns or 3200 ns is enabled for IEEE 802.11ax physical layer parameters of a bandwidth of 20 MHz and 2 spatial streams	47

5.4 Simulated packet error rate (PER) in regards to Signal Noise Ratio (SNR) for chosen HE-MCS values and whether DCM is enabled for IEEE 802.11ax physical layer parameters of a GI of 3200 ns, a Bandwidth (BW) of 20 MHz and 2 spatial streams	48
5.5 Simulated packet error rate (PER) in regards to Signal Noise Ratio (SNR) for chosen HE-MCS values and whether Extended Range or DCM is enabled for IEEE 802.11ax physical layer parameters of a GI of 3200 ns, a Bandwidth (BW) of 20 MHz and 2 spatial streams	49
5.6 Simulated packet error rate (PER) in regards to Signal Noise Ratio (SNR) for chosen HE-MCS values and whether STBC is enabled for IEEE 802.11ax physical layer parameters of a GI of 3200 ns, a Bandwidth (BW) of 20 MHz and 2 spatial streams	50
5.7 Achieved Goodput and theoretical Datarate of two Wi-Fi6 stations in Ad-Hoc Mode with 2 Multiple Input Multiple Output (MIMO) streams and a bandwidth of 80 MHz in regards to the chosen Guard Interval (GI) and HE-MCS value	55
5.8 Achieved Goodput and theoretical Datarate of two Wi-Fi6 stations in Ad-Hoc Mode with a Guard Interval (GI) of 3200 ns and a bandwidth of 20 MHz in regards to the number of Multiple Input Multiple Output (MIMO) streams and the chosen HE-MCS value	57
5.9 Achieved Goodput and theoretical Datarate of two Wi-Fi6 stations in Ad-Hoc Mode with for IEEE 802.11ax physical layer parameters of a Guard Interval (GI) of 3200 ns, a Bandwidth (BW) of 20 MHz and 2 spatial streams in regards to the number of the chosen HE-Modulation and Coding Scheme (MCS) value and whether Dual Carrier Modulation (DCM) is enabled	58
5.10 Achieved Goodput and theoretical Datarate of two IEEE 802.11ax stations in Ad-Hoc Mode with for IEEE 802.11ax physical layer parameters of a Guard Interval (GI) of 3200 ns, a Bandwidth (BW) of 20 MHz and 2 spatial streams in regards to the number of the chosen HE-Modulation and Coding Scheme (MCS) value and whether Space-Time-Block-Code (STBC) is enabled	59
6.1 Path of the Forage Harvester (FH) for harvesting corn on the field . .	64
6.2 Start position of the Forage Harvester (FH)s and Transport Machine (TM)s, where a FH broadcasts a search request to find a TM to load the corn onto	64
6.3 Markov Chain for the Harvest States 0, 1 and 2, which represent the current Plant Density (PD) and harvest speed from Table 6.2	66

6.4 Transport Machine (TM) position left of the Forage Harvester (FH) for overloading, where the TM is half full and the FH starts Algorithm 6.1 to search for a next empty TM, which can later take over the loading position.	67
6.5 Change of Transport Machine (TM)s in the Application Agricultural Platooning Service, where TM_1 is full and leaves the field while the empty TM_2 takes over the overloading position.	68
6.6 Screenshot of the simulation visualization in Netsimulyzer, where a blue Transport Machine (TM) is unloading in the back in front of the farm cuboid, two red TMs are in a Agricultural Platooning Service with the black Forage Harvester (FH)s, a green TM is empty and waiting for a new <i>search_TM</i> request and a yellow TM is in waiting position behind a black FH.	69
6.7 Mean latency and mean guidance data update interval of the Application Agricultural Platooning Service in regards to the number of FHs and TMs and the chosen HE-MCS value for a <i>platoon_data_interval</i> of 50 ms.	71
6.8 Mean latency and mean guidance data update interval of the Application Agricultural Platooning Service in regards to the number of FHs and TMs and the chosen HE-MCS value for a <i>platoon_data_interval</i> of 25 ms.	72

List of Tables

2.1	Key figures of corn harvest of a Forage Harvester (FH) with a working width of 6.2 m in a 80 ha-field in regards to Plant Density (PD) calculated from [7]	6
2.2	Available Bandwidth (BW)s for the IEEE 802.11 standards per frequency band.	10
2.3	MCS and Coding Rate (CR) for HE-MCS values [16]	12
2.4	Access Categories and their priorities for IEEE 802.11e Enhanced Distributed Channel Access (EDCA) [38]	18
4.1	Frequency channel numbers for 2.4 GHz and 5 GHz for the different Bandwidth (BW)s of the IEEE 802.11 standard [16], which can be used for outdoor communication [54], [55] and can be configured in the Milesight Industrial Router UR75 for the field experiments.	34
5.1	Default physical layer settings for the IEEE 802.11ax robustness simulations	42
5.2	Default simulation parameters for Wi-Fi Devices in the goodput simulations	53
5.3	Bandwidth (BW) attenuation and mean goodput for HE-MCS0 in regards to Guard Interval (GI) length	55
6.1	Default simulation parameters for Wi-Fi Devices on Forage Harvester (FH) and Transport Machine (TM)	63
6.2	Corn harvest states, which define a range of Plant Density (PD)s and Forage Harvester (FH) speeds, where the data is based on the key figures [7]	66
6.3	Simulation parameters for the Application Agricultural Platooning Service	68

6.4 Corn harvest states, which define a range of Plant Density (PD)s from [7] and Forage Harvester (FH) speeds, which I set higher than the key figures in [7] specify to increase the requirements on the Agricultural Platooning Service.	71
--	----

Bibliography

- [1] N. Iglesias, P. Bulacio, and E. Tapia, “Enabling powerful GUIs in ISOBUS networks by transparent data compression,” *Computer Standards & Interfaces*, vol. 36, no. 5, pp. 801–807, Sep. 2014. doi: <https://doi.org/10.1016/j.csi.2014.01.007>.
- [2] N. Schlingmann and M. Benishek, “AEF - Providing electronic communication to the Ag sector for Wireless In - Field Communication,” in *2019 ASABE Annual International Meeting*, Boston, USA: American Society of Agricultural and Biological Engineers, Jul. 2019. doi: 10.13031/aim.201901864.
- [3] N. Schlingmann, H. Schallermayer, J. Witte, and C. Gossard, “Challenges of digital revolution – How the AEF plans to manage interoperability,” in *VDI-Berichte: LAND.TECHNIK AgEng 2017*, vol. 2300, VDI Verlag, 2017, pp. 477–484. doi: 10.51202/9783181023006-477.
- [4] “ICT Facts and Figures 2016,” ITU, ITU-D ICT Statistics 2016, 2016.
- [5] “Use of the 5.850-5.925 GHz Band,” Federal Communications Commission, Rule 2021-08802, May 2021.
- [6] H. Seifert, K. Grimm, and M. Schurig, *Der Feldhäcksler und was dazu gehört* (KTL - Flugschrift Kuratorium für Technik in der Landwirtschaft), de. Wolfratshausen bei München: Hellmut-Neureuter-Verlag, 1962, vol. 10, ISSN: 0452-8948.
- [7] Faustzahlen für die Landwirtschaft, ger, 15. Aufl. Darmstadt: Kuratorium für Technik und Bauwesen in der Landwirtschaft e.V. (KTBL), 2018.
- [8] X. Zhang, M. Geimer, L. Grandl, and B. Kammerbauer, “Method for an electronic controlled platooning system of agricultural vehicles,” in *2009 IEEE International Conference on Vehicular Electronics and Safety (ICVES)*, Pune, India: IEEE, Nov. 2009, pp. 156–161. doi: 10.1109/ICVES.2009.5400187.
- [9] Z. Liu, S. Dhamankar, J. T. Evans, C. M. Allen, C. Jiang, G. M. Shaver, A. Etienne, T. J. Vyn, C. M. Puryk, and B. M. McDonald, “Automation of Agricultural Grain Unloading-on-the-go,” en, *IFAC-PapersOnLine*, 10th IFAC Symposium

- on Advances in Automotive Control AAC 2022, vol. 55, no. 24, pp. 248–253, Oct. 2022. DOI: 10.1016/j.ifacol.2022.10.292.
- [10] “Arbeitskräfte in der Landwirtschaft / BMEL (723),” Statistisches Bundesamt: Fachserie 3, BMEL (723) Reihe 2.1.8, 2020, <https://www.bmel-statistik.de/landwirtschaft/landwirtschaftliche-arbeitskraefte>.
- [11] I. Smolnik and A. Lücke, “5G NetMobil - 5G Lösungen für die vernetzte Mobilität der Zukunft : Schlussbericht : Teilvorhaben: "Entwicklung eines Parallelen Platooning Systems für den Bereich der Landtechnik unter Verwendung von 5G Technologien" - Schlussbericht,” Claas E-Systems GmbH, Dissen , Germany, Tech. Rep., 2020, p. 47. DOI: 10.2314/KXP:1757666915.
- [12] H. Murcia, “A quadrotor as remote sensor for on-line profile measurement during harvesting process,” Ph.D. dissertation, May 2014. DOI: 10.13140/RG.2.1.1842.3522.
- [13] F.-J. Kauffels, Wireless LANs: drahtlose Netze planen und verwirklichen, der Standard IEEE 802.11 im Detail, WLAN-Design und Sicherheitsrichtlinien (Netzwerke), ger, 1. Aufl. Bonn: mitp-Verl, 2002.
- [14] M. Sauter, “Wireless LAN IEEE 802.11,” de, in *Grundkurs Mobile Kommunikationssysteme: 5G New Radio und Kernnetz, LTE-Advanced Pro, GSM, Wireless LAN und Bluetooth*, M. Sauter, Ed., Wiesbaden: Springer Fachmedien, 2022, pp. 265–338. DOI: 10.1007/978-3-658-36963-7_4.
- [15] “IEEE Standard for Information Technology—Telecommunications and Information Exchange between Systems - Local and Metropolitan Area Networks—Specific Requirements - Part 11: Wireless LAN Medium Access Control (MAC) and Physical Layer (PHY) Specifications,” *IEEE Std 802.11-2020 (Revision of IEEE Std 802.11-2016)*, pp. 1–4379, Feb. 2021, Conference Name: IEEE Std 802.11-2020 (Revision of IEEE Std 802.11-2016). DOI: 10.1109/IEEESTD.2021.9363693.
- [16] “IEEE Standard for Information Technology—Telecommunications and Information Exchange between Systems Local and Metropolitan Area Networks—Specific Requirements Part 11: Wireless LAN Medium Access Control (MAC) and Physical Layer (PHY) Specifications Amendment 1: Enhancements for High-Efficiency WLAN,” *IEEE Std 802.11ax-2021 (Amendment to IEEE Std 802.11-2020)*, pp. 1–767, May 2021, Conference Name: IEEE Std 802.11ax-2021 (Amendment to IEEE Std 802.11-2020). DOI: 10.1109/IEEESTD.2021.9442429.

- [17] R. Jacob, W. Anwar, N. Schwarzenberg, N. Franchi, and G. Fettweis, "System-level Performance Comparison of IEEE 802.11p and 802.11bd Draft in Highway Scenarios," en, in *2020 27th International Conference on Telecommunications (ICT)*, Bali, Indonesia: IEEE, Oct. 2020, pp. 1–6. DOI: 10.1109/ICT49546.2020.9239538.
- [18] S. Avallone, P. Imputato, G. Redieteab, C. Ghosh, and S. Roy, "Will OFDMA Improve the Performance of 802.11 Wifi Networks?" *IEEE Wireless Communications*, vol. 28, no. 3, pp. 100–107, Jun. 2021, Conference Name: IEEE Wireless Communications. DOI: 10.1109/MWC.001.2000332.
- [19] M. S. Afiaqui, E. Garcia-Villegas, and E. Lopez-Aguilera, "IEEE 802.11ax: Challenges and Requirements for Future High Efficiency WiFi," *IEEE Wireless Communications*, vol. 24, no. 3, pp. 130–137, Jun. 2017, Conference Name: IEEE Wireless Communications. DOI: 10.1109/MWC.2016.1600089WC.
- [20] W. A. Syafei, R. Yohena, H. Shimajiri, T. Yoshida, M. Kurosaki, Y. Nagao, B. Sai, and H. Ochi, "Performance Evaluation and ASIC Design of LDPC Decoder for IEEE802.11n," in *2009 6th IEEE Consumer Communications and Networking Conference*, ISSN: 2331-9860, Las Vegas, USA: IEEE, Jan. 2009, p. 5. DOI: 10.1109/CCNC.2009.4784735.
- [21] B. Y. Yacheur, T. Ahmed, and M. Mosbah, "Analysis and Comparison of IEEE 802.11p and IEEE 802.11bd," en, in *Communication Technologies for Vehicles*, F. Krief, H. Aniss, L. Mendiboure, S. Chaumette, and M. Berbineau, Eds., vol. 12574, Series Title: Lecture Notes in Computer Science, Cham: Springer International Publishing, 2020, pp. 55–65. DOI: 10.1007/978-3-030-66030-7_5.
- [22] N. Pulimamidi, J. Nulu, and M. M. Tahernezhadi, "Development of a new OFDM transceiver without guard interval," in *2007 IEEE International Conference on Electro/Information Technology*, ISSN: 2154-0373, Chicago, USA: IEEE, May 2007, pp. 300–305. DOI: 10.1109/EIT.2007.4374539.
- [23] N. S. Ravindranath, I. Singh, A. Prasad, and V. S. Rao, "Performance Evaluation of IEEE 802.11ac and 802.11n using NS3," en, *Indian Journal of Science and Technology*, vol. 9, no. 26, p. 9, Jul. 2016. DOI: 10.17485/ijst/2016/v9i26/93565.
- [24] Van Duc Nguyen and H.-P. Kuchenbecker, "Intercarrier and intersymbol interference analysis of OFDM systems on time-invariant channels," en, in *The 13th IEEE International Symposium on Personal, Indoor and Mobile Radio Communications*, vol. 4, Lisbon, Portugal: IEEE, 2002, pp. 1482–1487. DOI: 10.1109/PIMRC.2002.1045425.

- [25] D.-J. Deng, Y.-P. Lin, X. Yang, J. Zhu, Y.-B. Li, J. Luo, and K.-C. Chen, “IEEE 802.11ax: Highly Efficient WLANs for Intelligent Information Infrastructure,” *IEEE Communications Magazine*, vol. 55, no. 12, pp. 52–59, Dec. 2017. doi: 10.1109/MCOM.2017.1700285.
- [26] A. F. Rochim, B. Harijadi, Y. P. Purbanugraha, S. Fuad, and K. A. Nugroho, “Performance comparison of wireless protocol IEEE 802.11ax vs 802.11ac,” in *2020 International Conference on Smart Technology and Applications (ICoSTA)*, Surabaya, Indonesia: IEEE, Feb. 2020, p. 5. doi: 10.1109/ICoSTA48221.2020.91570609404.
- [27] E. Mozaffariahrar, F. Theoleyre, and M. Menth, “A Survey of Wi-Fi 6: Technologies, Advances, and Challenges,” en, *Future Internet*, vol. 14, no. 10, p. 293, Oct. 2022, Publisher: Multidisciplinary Digital Publishing Institute. doi: 10.3390/fi14100293.
- [28] A. Triwinarko, I. Dayoub, and S. Cherkaoui, “PHY layer enhancements for next generation V2X communication,” en, *Vehicular Communications*, vol. 32, p. 100385, Dec. 2021. doi: 10.1016/j.vehcom.2021.100385.
- [29] H. A. Omar, K. Abboud, N. Cheng, K. R. Malekshan, A. T. Gamage, and W. Zhuang, “A Survey on High Efficiency Wireless Local Area Networks: Next Generation WiFi,” *IEEE Communications Surveys & Tutorials*, vol. 18, no. 4, pp. 2315–2344, 2016, Conference Name: IEEE Communications Surveys & Tutorials. doi: 10.1109/COMST.2016.2554098.
- [30] E. Khorov, A. Kiryanov, A. Lyakhov, and G. Bianchi, “A Tutorial on IEEE 802.11ax High Efficiency WLANs,” *IEEE Communications Surveys & Tutorials*, vol. 21, no. 1, pp. 197–216, Sep. 2019, Publisher: IEEE. doi: 10.1109/COMST.2018.2871099.
- [31] A. Behara and T. Venkatesh, “Performance Study of High-Efficiency IEEE 802.11ax WLAN Standard Using NS-3 Simulator,” in *2022 IEEE 27th International Workshop on Computer Aided Modeling and Design of Communication Links and Networks (CAMAD)*, ISSN: 2378-4873, Paris, France: IEEE, Nov. 2022, pp. 226–231. doi: 10.1109/CAMAD55695.2022.9966905.
- [32] W. Abbas, N. Abbas, U. Majeed, and S. Khan, “EFFICIENT STBC FOR THE DATA RATE OF MIMO-OFDMA,” en, *Science International Journal*, vol. 24, pp. 247–255, Jan. 2016.
- [33] S. Santumon and B. Sujatha, “Space-Time Block Coding (STBC) for Wireless Networks,” en, *International Journal of Distributed and Parallel systems*, vol. 3, no. 4, pp. 183–195, Jul. 2012. doi: 10.5121/ijdps.2012.3419.

- [34] A. Stamoulis and N. Al-Dhahir, "Impact of space-time block codes on 802.11 network throughput," en, *IEEE Transactions on Wireless Communications*, vol. 2, no. 5, pp. 1029–1039, Sep. 2003. DOI: 10.1109/TWC.2003.816798.
- [35] P. K. Ghosh, Manju, K. Gupta, and B. Dey, "Error analysis of multiple rate space-time-block-code (STBC) for MIMO networks," in *Proceedings of The 2014 International Conference on Control, Instrumentation, Energy and Communication (CIEC)*, Calcutta, India: IEEE, Jan. 2014, pp. 691–695. DOI: 10.1109/CIEC.2014.6959179.
- [36] M. S. Gast, 802.11n: A Survival Guide, en. O'Reilly Media, Inc., Apr. 2012.
- [37] C. Sommer and F. Dressler, Vehicular Networking. Cambridge: Cambridge University Press, 2014. DOI: 10.1017/CBO9781107110649.
- [38] H. Wu, X. Wang, Q. Zhang, and X. Shen, "IEEE 802.11e Enhanced Distributed Channel Access (EDCA) Throughput Analysis," in *2006 IEEE International Conference on Communications*, ISSN: 1938-1883, Istanbul, Turkey: IEEE, Jun. 2006, pp. 223–228. DOI: 10.1109/ICC.2006.254731.
- [39] "IEEE Standard for Information technology– Local and metropolitan area networks– Specific requirements– Part 11: Wireless LAN Medium Access Control (MAC)and Physical Layer (PHY) Specifications Amendment 5: Enhancements for Higher Throughput," *IEEE Std 802.11n-2009 (Amendment to IEEE Std 802.11-2007 as amended by IEEE Std 802.11k-2008, IEEE Std 802.11r-2008, IEEE Std 802.11y-2008, and IEEE Std 802.11w-2009)*, pp. 1–565, Oct. 2009, Conference Name: IEEE Std 802.11n-2009 (Amendment to IEEE Std 802.11-2007 as amended by IEEE Std 802.11k-2008, IEEE Std 802.11r-2008, IEEE Std 802.11y-2008, and IEEE Std 802.11w-2009). DOI: 10.1109/IEEESTD.2009.5307322.
- [40] "IEEE Standard for Information technology– Local and metropolitan area networks– Specific requirements– Part 11: Wireless LAN Medium Access Control (MAC) and Physical Layer (PHY) Specifications Amendment 6: Wireless Access in Vehicular Environments," *IEEE Std 802.11p-2010 (Amendment to IEEE Std 802.11-2007 as amended by IEEE Std 802.11k-2008, IEEE Std 802.11r-2008, IEEE Std 802.11y-2008, IEEE Std 802.11n-2009, and IEEE Std 802.11w-2009)*, pp. 1–51, Jul. 2010, Conference Name: IEEE Std 802.11p-2010 (Amendment to IEEE Std 802.11-2007 as amended by IEEE Std 802.11k-2008, IEEE Std 802.11r-2008, IEEE Std 802.11y-2008, IEEE Std 802.11n-2009, and IEEE Std 802.11w-2009). DOI: 10.1109/IEEESTD.2010.5514475.
- [41] K. Lautenschlaeger and C. Sommer, "Beyond Sensing: Suitability of LoRa for Meshed Automatic Section Control of Agricultural Vehicles," in *2022 17th Wireless On-Demand Network Systems and Services Conference (WONS)*,

- Oppdal, Norway: IEEE, Mar. 2022, pp. 1–4. doi: 10.23919/WONS54113.2022.9764458.
- [42] O. Ali, B. Saint Germain, J. Van Belle, P. Valckenaers, H. Van Brussel, and J. Van Noten, “Multi-agent coordination and control system for multi-vehicle agricultural operations,” in *Proc. of 9th Int. Conf. on Autonomous Agents and Multiagent Systems (AAMAS 2010)*, vol. 3, Toronto, Canada: International Foundation for Autonomous Agents and Multiagent Systems (IFAAMAS), May 2010, pp. 1621–1622.
- [43] F. Klingler, J. Blobel, and F. Dressler, “Agriculture meets IEEE 802.11p: A Feasibility Study,” in *2018 15th International Symposium on Wireless Communication Systems (ISWCS)*, Lisbon, Portugal: IEEE, Aug. 2018. doi: 10.1109/ISWCS.2018.8491239.
- [44] J. A. Thomasson, C. P. Baillie, D. L. Antille, C. L. McCarthy, and C. R. Lobsey, “A review of the state of the art in agricultural automation. Part II: On-farm agricultural communications and connectivity,” en, in *2018 ASABE Annual International Meeting*, Paper No.: 1801590, American Society of Agricultural and Biological Engineers (ASABE), 2018. doi: 10.13031/aim.201801590.
- [45] P. Metzler, W. Flohr, and M. Hoeh, “System for determining the relative position of a second farm vehicle in relation to a first farm vehicle,” DE102004039460 (B3) ■ Apr. 2006.
- [46] N. Ahmed, D. De, and I. Hussain, “Internet of Things (IoT) for Smart Precision Agriculture and Farming in Rural Areas,” *IEEE Internet of Things Journal*, vol. 5, no. 6, pp. 4890–4899, Nov. 2018, Conference Name: IEEE Internet of Things Journal. doi: 10.1109/JIOT.2018.2879579.
- [47] J. Brinkhoff and J. Hornbuckle, “Characterization of WiFi signal range for agricultural WSNs,” in *2017 23rd Asia-Pacific Conference on Communications (APCC)*, Perth, Australia: IEEE, Dec. 2017, pp. 1–6. doi: 10.23919/APCC.2017.8304043.
- [48] S. Aust, R. V. Prasad, and I. G. M. M. Niemegeers, “Outdoor Long-Range WLANs: A Lesson for IEEE 802.11ah,” *IEEE Communications Surveys & Tutorials*, vol. 17, no. 3, pp. 1761–1775, 2015, Conference Name: IEEE Communications Surveys & Tutorials. doi: 10.1109/COMST.2015.2429311.
- [49] A. Sheth, S. Nedevschi, R. Patra, S. Surana, E. Brewer, and L. Subramanian, “Packet Loss Characterization in WiFi-Based Long Distance Networks,” in *IEEE INFOCOM 2007 - 26th IEEE International Conference on Computer Communications*, ISSN: 0743-166X, Anchorage, AK, USA: IEEE, May 2007, pp. 312–320. doi: 10.1109/INFCOM.2007.44.

- [50] D. Aguayo, J. Bicket, S. Biswas, G. Judd, and R. Morris, “Link-level measurements from an 802.11b mesh network,” vol. 34, Portland Oregon USA: Association for Computing Machinery, Aug. 2004, pp. 121–132. DOI: 10.1145/1030194.1015482.
- [51] K. Chebrolu, B. Raman, and S. Sen, “Long-distance 802.11b links: performance measurements and experience,” in *MobiCom '06: Proceedings of the 12th annual international conference on Mobile computing and networking*, ser. MobiCom '06, Los Angeles CA USA: Association for Computing Machinery, Sep. 2006, pp. 74–85. DOI: 10.1145/1161089.1161099.
- [52] U. Paul, R. Crepaldi, J. Lee, S.-J. Lee, and R. Etkin, “Characterizing WiFi link performance in open outdoor networks,” in *2011 8th Annual IEEE Communications Society Conference on Sensor, Mesh and Ad Hoc Communications and Networks*, ISSN: 2155-5494, Salt Lake City, USA: IEEE, Jun. 2011, pp. 251–259. DOI: 10.1109/SAHCN.2011.5984905.
- [53] A. Nedelcu, R. Ciuperca, A. Zaica, and V. Stefan, “Influence of forage harvester chopping equipment on characteristics of chips,” en, in *Proceedings of 19th International Scientific Conference Engineering for Rural Development*, Jelgava, Latvia, May 2020. DOI: 10.22616/ERDev.2020.19.TF330.
- [54] “Allgemeinzuteilung von Frequenzen für die Nutzung in lokalen Netzwerken; Wireless Local Area Networks (WLAN-Funkanwendungen),” Bundesnetzagentur, Vfg. 136 / 2022, <https://www.bundesnetzagentur.de> -> Fachthemen -> Telekommunikation -> Funk und Frequenzen -> Allgemeinzuteilungen -> WLAN.
- [55] “Allgemeinzuteilung von Frequenzen in den Bereichen 5150 MHz - 5250 MHz, 5250 - 5350 MHz und 5470 MHz - 5725 MHz für drahtloser Zugangssysteme einschließlich lokaler Funknetze (WAS/Funk-LANs),” Bundesnetzagentur, Vfg. 136 / 2022, Nov. 2022, <https://www.bundesnetzagentur.de> -> Fachthemen -> Telekommunikation -> Funk und Frequenzen -> Allgemeinzuteilungen -> WLAN.
- [56] “IEEE Standard for Telecommunications and Information Exchange Between Systems - LAN/MAN Specific Requirements - Part 11: Wireless Medium Access Control (MAC) and physical layer (PHY) specifications: High Speed Physical Layer in the 5 GHz band,” *IEEE Std 802.11a-1999*, pp. 1–102, Dec. 1999, Conference Name: IEEE Std 802.11a-1999. DOI: 10.1109/IEEESTD.1999.90606.
- [57] A. Kumar, S. K. Kaushik, R. Sharma, and P. Raj, “Simulators for Wireless Networks: A Comparative Study,” in *2012 International Conference on Computing*

- Sciences*, Phagwara, India: IEEE, Sep. 2012, pp. 338–342. DOI: 10.1109/ICCS.2012.65.
- [58] S. C. Sheela, J. Kuri, and N. Akhtar, “Performance Analysis of Channel-Dependent Rate Adaptation for OFDMA transmission in IEEE 802.11ax WLANs,” in *2022 14th International Conference on COMmunication Systems & NETworkS (COMSNETS)*, ISSN: 2155-2509, Bangalore, India: IEEE, Jan. 2022, pp. 877–882. DOI: 10.1109/COMSNETS53615.2022.9668513.
- [59] L. Cao, L. Zhang, S. Jin, and S. Roy, Efficient PHY Layer Abstraction under Imperfect Channel Estimation, arXiv:2205.10897 [eess], Oct. 2022. DOI: 10.48550/arXiv.2205.10897.
- [60] S. Jin, S. Roy, and T. R. Henderson, “Efficient PHY Layer Abstraction for Fast Simulations in Complex System Environments,” *IEEE Transactions on Communications*, vol. 69, no. 8, pp. 5649–5660, Aug. 2021. DOI: 10.1109/TCOMM.2021.3079285.
- [61] “IEEE 802.11ax Channel Model Document,” IEEE, TGAX channel model document, Sep. 2014, IEEE 802.11-14/0882r4.
- [62] T. H. Tran, Y. Nagao, H. Ochi, and M. Kuroasaki, “ASIC design of 7.7 Gbps multi-mode LDPC decoder for IEEE 802.11ac,” in *2014 14th International Symposium on Communications and Information Technologies (ISCIT)*, Incheon, South Korea: IEEE, Sep. 2014, pp. 259–263. DOI: 10.1109/ISCIT.2014.7011912.
- [63] P. Patil, M. Patil, S. Itraj, and U. Bombale, “IEEE 802.11n: Joint modulation-coding and guard interval adaptation scheme for throughput enhancement,” in *International Journal of Communication Systems*, vol. 33, no. 8, e4347, Feb. 2020, _eprint: <https://onlinelibrary.wiley.com/doi/pdf/10.1002/dac.4347>. DOI: 10.1002/dac.4347.
- [64] E. Khorov, A. Kiryanov, and A. Lyakhov, “IEEE 802.11ax: How to Build High Efficiency WLANs,” in *2015 International Conference on Engineering and Telecommunication (EnT)*, Moscow, Russia: IEEE, Nov. 2015, pp. 14–19. DOI: 10.1109/EnT.2015.23.
- [65] H.-S. Ryu, J.-S. Lee, and C. G. Kang, “BER analysis of dual-carrier modulation (DCM) over Rayleigh fading channel,” in *International Congress on Ultra Modern Telecommunications and Control Systems*, ISSN: 2157-023X, Moscow, Russia: IEEE, Oct. 2010, pp. 717–721. DOI: 10.1109/ICUMT.2010.5676558.
- [66] K.-h. Park, H.-k. Sung, and Y.-c. Ko, “BER Analysis of Dual Carrier Modulation Based on ML Decoding,” in *2006 Asia-Pacific Conference on Communications*, ISSN: 2163-0771, Busan, South Korea: IEEE, Aug. 2006, p. 4. DOI: 10.1109/APCC.2006.255858.

- [67] V. Tarokh, H. Jafarkhani, and A. Calderbank, “Space-time block codes from orthogonal designs,” *IEEE Transactions on Information Theory*, vol. 45, no. 5, pp. 1456–1467, Jul. 1999, Conference Name: IEEE Transactions on Information Theory. DOI: 10.1109/18.771146.
- [68] J. A. Shaw, “Radiometry and the Friis transmission equation,” *American Journal of Physics*, vol. 81, no. 1, pp. 33–37, Dec. 2012, Publisher: American Association of Physics Teachers. DOI: 10.1119/1.4755780.
- [69] S. Keller, J. Andre, and F. Wiedner, “Simulation of WiFi Mesh Networks with Mobile Nodes,” en, *Network Architectures and Services Seminar IITM SS 21*, p. 4, Nov. 2021, Publisher: Chair of Network Architectures and Services, Department of Computer Science, Technical University of Munich. DOI: 10.2313/NET-2022-01-1_01.
- [70] T. Henderson, ns-3-dev, Software Gitrepository ns-3-dev, version 3.37, Mar. 2023.
- [71] E. Black, S. Gamboa, and R. Rouil, “NetSimulyzer: a 3D network simulation analyzer for ns-3,” en, in *Proceedings of the Workshop on ns-3*, Virtual Event USA: ACM, Jun. 2021, pp. 65–72. DOI: 10.1145/3460797.3460806.
- [72] I. Dolińska, M. Jakubowski, and A. Masiukiewicz, “New IEEE 802.11 HEW Standard Throughput per User Analysis,” in *2019 International Conference on Information and Digital Technologies (IDT)*, ISSN: 2575-677X, Zilina, Slovakia: IEEE, Jun. 2019, pp. 118–123. DOI: 10.1109/DT.2019.8813700.
- [73] R. Karmakar, S. De, A. Ghosh, T. Adhikari, and P. Jain, “S2-GI: Intelligent Selection of Guard Interval in High Throughput WLANs,” in *2020 11th International Conference on Computing, Communication and Networking Technologies (ICCCNT)*, Kharagpur, India: IEEE, Jul. 2020, p. 7. DOI: 10.1109/ICCCNT49239.2020.9225322.
- [74] “Study on enhancement of 3GPP Support for 5G V2X Services (Release 16),” 3GPP, TR TR 22.886, version 16.2.0, Dec. 2018.

Todo list

 Ref: Photograph from CLAAS KGaA mbH	5
 What is LLC? Logic Link Control?	16
 add sources	17
 Einordnen in andere Scenarios	31
 Ground reflection coefficient beton grass, permeability, conductance, permittivity of grass, permittivity of concrete, permittivity of air, permittivity of water	39